HYDRAULICS BRANCH
OFFICIAL FILE COPY

PAP-477

BUREAU OF RECLAMATION
HYDRAULICS BRANCH

OFFICE FILE COPY

** When Borrowed, Return Promptly **

MODEL INVESTIGATION ON VIBRATION OF THE DEEP-WATER GATE IN TOUTUN RIVER RESERVOIR IN IN XINGJIANG

BY

YAN SHIWU

PAP-477

United States Department of the Interior
Bureau of Reclamation
Engineering and Research Center

Translation No. 1928
Team No. General
Book No. 12,524

XXXXXXXXXXXXXXXXXXXXXXXXXXXXXXXXXXXXXXXXXXXXXXXXXXXXXXXXXXXXXXXXXXXXXXXXXXXXXXXXXXX

MODEL INVESTIGATION ON VIBRATION OF THE DEEP-WATER GATE IN TOUTUN RIVER RESERVOIR IN XINGJIANG

Xingjiang toutunhe shuiku shenshuihumen
zhendongshiyan yanjiubaogao

by

Yan Shiwu

(*Nanjing Hydraulic Research Institute*)

Nanjing Shuilikexue Yanjiushuo

Shuilidianlibu

Jiaotongbu

1983

Translated from the Chinese: Research Reports, Nanjing Hydraulic Research Institute, Ministry of Water Conservancy and Electric Power, Ministry of Communication, 1983

Translated by Dr. David Hsu, Foreign Resources Associates

XXXXXXXXXXXXXXXXXXXXXXXXXXXXXXXXXXXXXXXXXXXXXXXXXXXXXXXXXXXXXXXXXXXXXXXXXXXXXXXXXXX

Division of Foreign Activities
Code D-2000

USBR Translations
Denver, Colorado
December 1984

Translation No.
Team No. General
Book No. 12,524

MODEL INVESTIGATION ON VIBRATION OF THE DEEP-WATER GATE IN TOUTUN RIVER RESERVOIR IN XINGJIANG

by

Yan Shiwu

ABSTRACT

This report describes an investigation on the working state of the tainter gate installed in the free-flow tunnel of the Toutun River Reservoir in Xingjiang. Reported here are results on the hydrodynamic pressure, free vibration characteristics of the gate system and the vibration under the action of hydrodynamic forces.

The report first gives the distribution curve of the time-averaged pressure and an empirical formula for the time-averaged total load:

$$P(a,H) = K(a) \cdot [H - h(a)] \qquad (2\text{-}7)$$

The energy spectral curves of the pressure fluctuation is then analyzed using the law of random functions. A preliminary analysis of the pulsating sources and the standard deviation of the pressure fluctuation, as well as the empirical formula for the flow conditions are then given. The following equations are given for calculating the mean pressure fluctuation and the fluctuating energy spectrum of the total load:

$$S_x(w) = \frac{1}{n^2} \sum_k \sum_j S_{xkj}(w) \qquad (3\text{-}15)$$

$$S_p(w) = \frac{A^2}{n^2} \sum_k \sum_j S_{xkj}(w) \qquad (3\text{-}16)$$

The report then proceeds to give a simple calculation diagram and the equation of motion for the principal vibration-prone components of the gate system and their free vibration frequencies.

Finally, the vibrations of the hanger rod of the lifter and support arms are calculated theoretically on the basis of the possible vibration modes of the gate system and the energy spectrum of the hydrodynamic force. The working condition of the gate system is related to the rod characteristics and the energy spectrum of the hydrodynamic forces. For the condition

studied here, both the hanger rod and support arm operate in the stable domain. The energy spectrum of their vibrating displacement and the bending and shear stresses are also calculated. Based on the results of the analysis, the gate system is considered dynamically stable under flow excitation.

Table of Contents

I. Introduction

The Toutun River Reservoir is located 8 km upstream from the August 1st Steel Mill in the suburb of Urumqi in Xingjiang. The main function of this general-purpose reservoir is to provide the industrial use of water; its secondary function is irrigation and flood control. The major projects are the main dam, concrete sluice tunnel, industrial water supply for the August 1st Steel Mill and the Hongyan reservoir inlet.

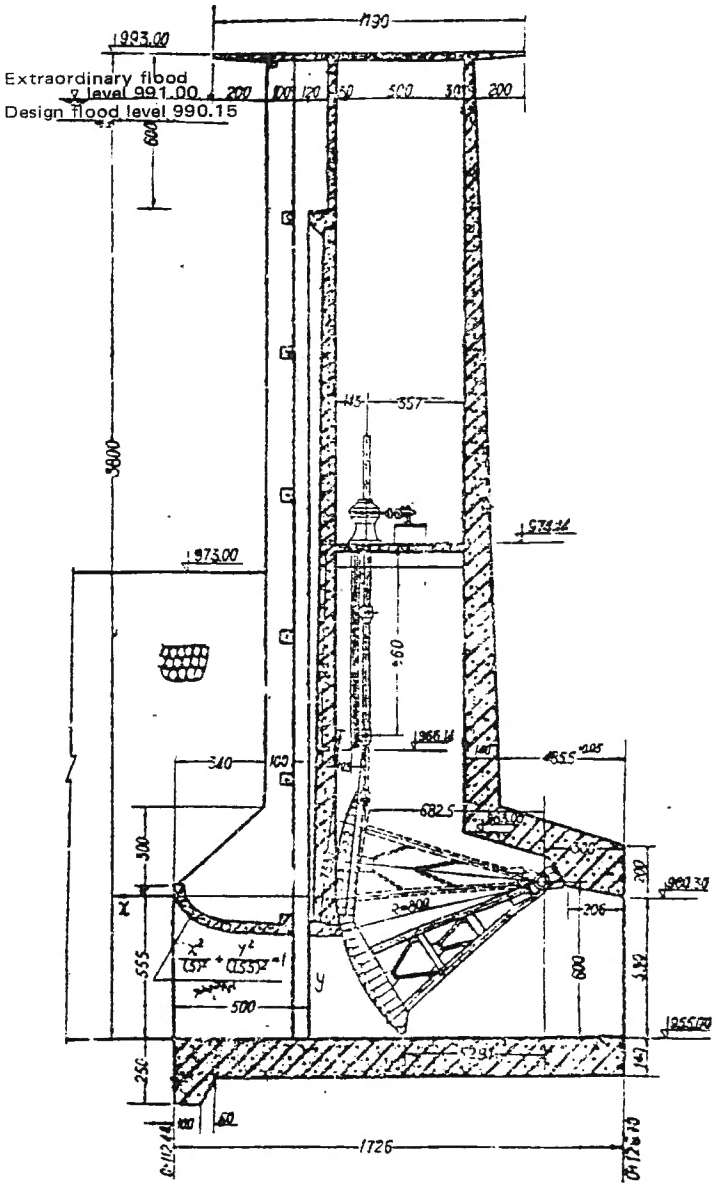

Figure 1. Cross-section of tunnel entrance.

In this study we address the vibration problem of the service gate in the sluice tunnel on the right bank of the reservoir. The tunnel has an open flow design, a water head of 35.16 m, flow capacity of 290 m^3/s, and total length of 450 m. The cross-section is flume-shaped in half-arc with straight walls measuring 5×5.3 m. A 4×4-m arc-shaped steel gate is installed at the entrance, as shown in Figure 1. The radius of the arc surface is 8 m, and the gate is operated by a Model 75/40 screw-type opener. The contracting agency wishes to answer the following questions:

1. The hydrodynamic pressure distribution at different open positions of the gate;
2. Vibration conditions at different open positions and discharge flow rates;
3. Possible resonance between the gate and the opener;
4. Suggestions to improve the design, operation and management.

II. Sluice capacity and time-averaged pressure load

(A) Model design

The model is designed on the basis of the gravitational similarity principle. Since the original design calls for an open flow, the model only contains the entrance section and a suitable length of the tunnel to reduce the construction work volume and yet satisfying the test requirements. The model has a normal design and scale of $L_r = 20$; hence, the flow-rate scale is $Q_r = L_r^{2.5} = 1800$, and the water-head scale is $H_r = L_r = 20$. With the exception of the bottom plate, the model is made of organic glass. The gate is made of galvanized sheet iron and replicates the actual shape. The time-averaged pressure is measured with pressure tubes at locations shown in Figure 2. The flow volume is measured with a rectangular weir. To simulate the actual situation, discharge volume and time-averaged pressure measurements are made for four different water levels (including the design water level and the calibration water level) and five different opening angles.

(B) Sluicing capacity

Under different water-level and gate-closure conditions no abnormal flow pattern is observed near the gate or in the conduit section. However, downstream from the gate the water surface is rough and there is evidence of a slight admix-

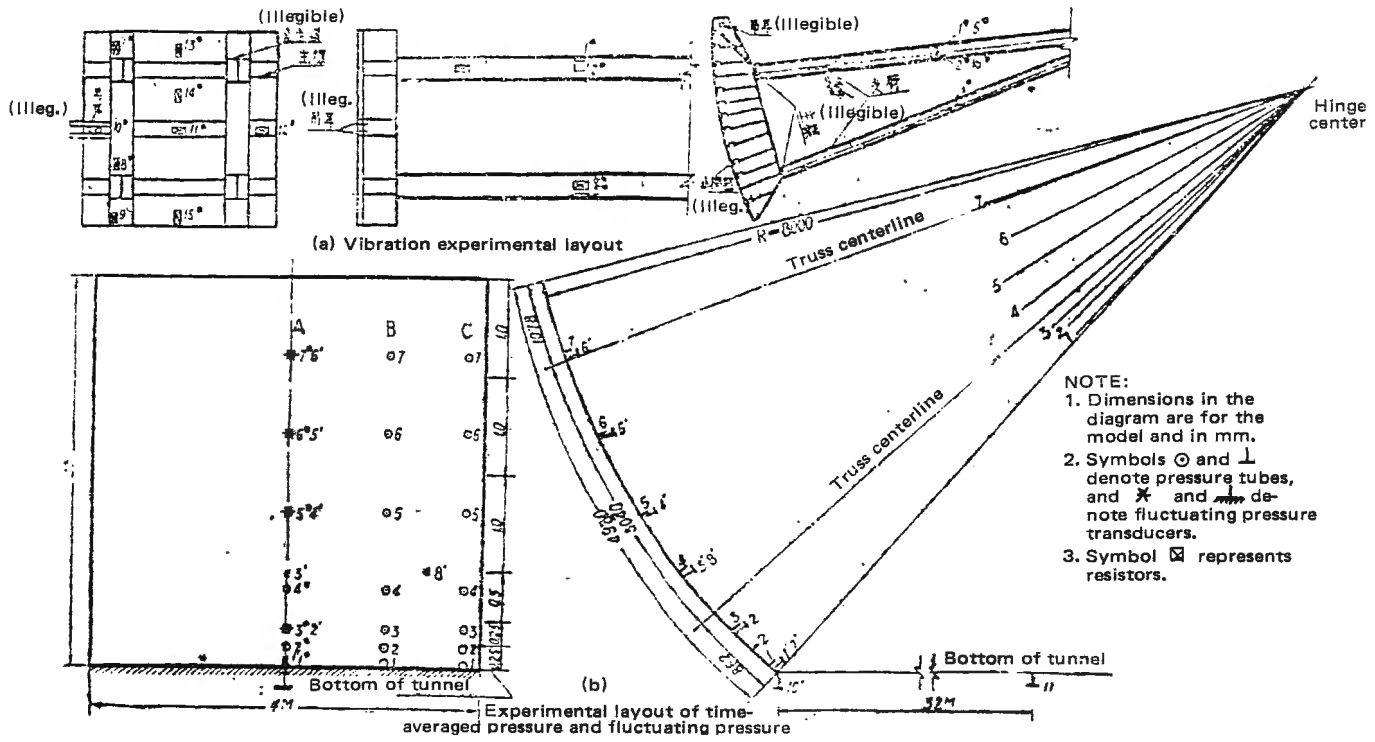

Figure 2. Layout of pressure measurement points.

ture of gas[a/], and shockwaves are observed in the conduit. The sluice conditions are shown in photographs 1 through 4, and the flow rate as a function of water level and gate closure is shown in Figure 3.

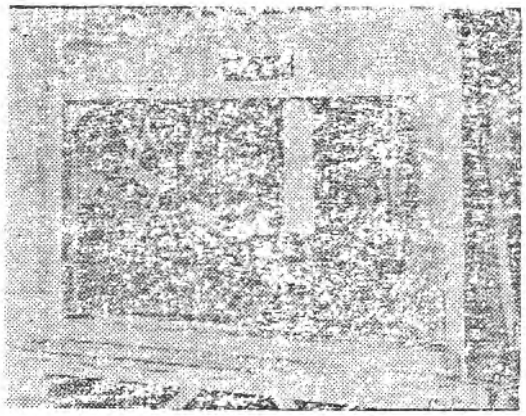

Photo 1

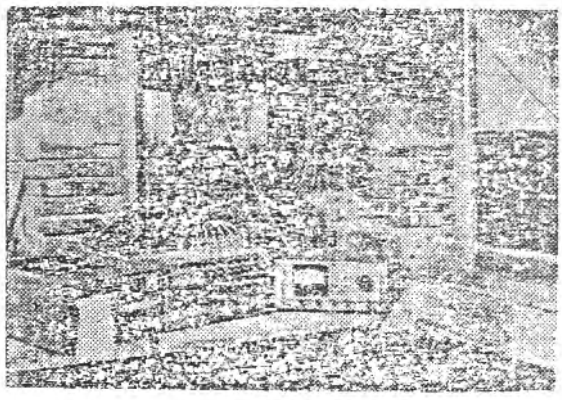

Photo 2

a/ The gas-admixture phenomenon is different in the model and in the prototype.

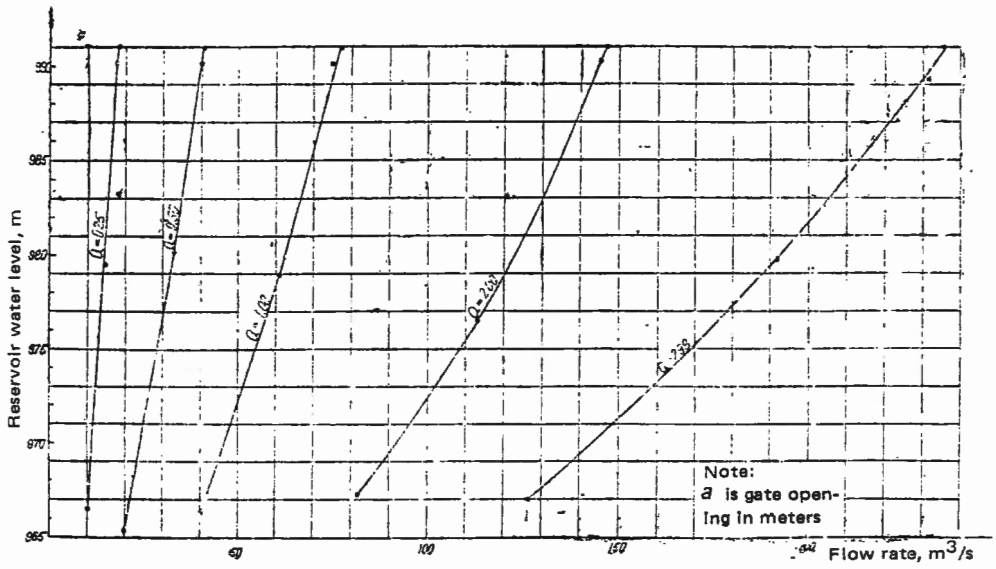

Figure 3. Water level—flow rate relationship.

(C) Time-averaged pressure load

The time-averaged pressure exerted on the face plate of the gate depends on the following parameters:

1. Physical dimensions of the opening and the gate (opening height a, opening width b, gate radius R, curvilinear distance S of the pressure-measuring opening to the bottom and the gate opening a_i);
2. Physical properties of the fluid (mass density ρ, gravitational acceleration g, and coefficient of viscosity ν);
3. Dynamic parameter (water head H — flow rate is also a function of water head).

Therefore, there exists the following functional relationship:

$$\varphi_1(a, b, R, s, a_i, H, p, \rho, g, \nu) = 0 \qquad (2\text{-}1)$$

Choosing P, a_i and ρ as the independent variables and invoking the π theorem, we have

$$\pi_1 = a/a_i; \quad \pi_2 = b/a_i; \quad \pi_3 = R/a_i; \quad \pi_4 = s/a_i; \quad \pi_5 = H/a_i; \quad \pi_6 = p/a_i r;$$

$$\pi_7 = \rho^{0.5}\nu/a_i\rho^{0.5}$$

and (2-1) may be rewritten as

$$\varphi_2(\pi_1,\ \pi_2,\ \pi_3,\ \pi_4,\ \pi_5,\ \pi_6,\ \pi_7) = 0 \qquad (2\text{-}2)$$

Obviously, the dimensionless number $\rho^{0.5}\nu/a_i p^{0.5}$ is related to the damping, and under normal circumstances may be regarded as a constant. Thus,

$$P/ra_i = \varphi_3\ (a/a_i,\ b/a_i,\ R/a_i,\ S/a_i,\ H/a_i) \qquad (2\text{-}3)$$

For a given gate, a , b and R are constants and, after some suitable substitution, (2-3) leads to the pressure distribution P:

$$P = \gamma ai\ \varphi_4(a/a_i,\ S/a_i,\ H/a_i) \qquad (2\text{-}4)$$

The time-averaged pressure curves P(a , H , s) in Figure 4 show that the pressure at any point on the gate increases as the water head increases, and decreases as the gate opening increases.

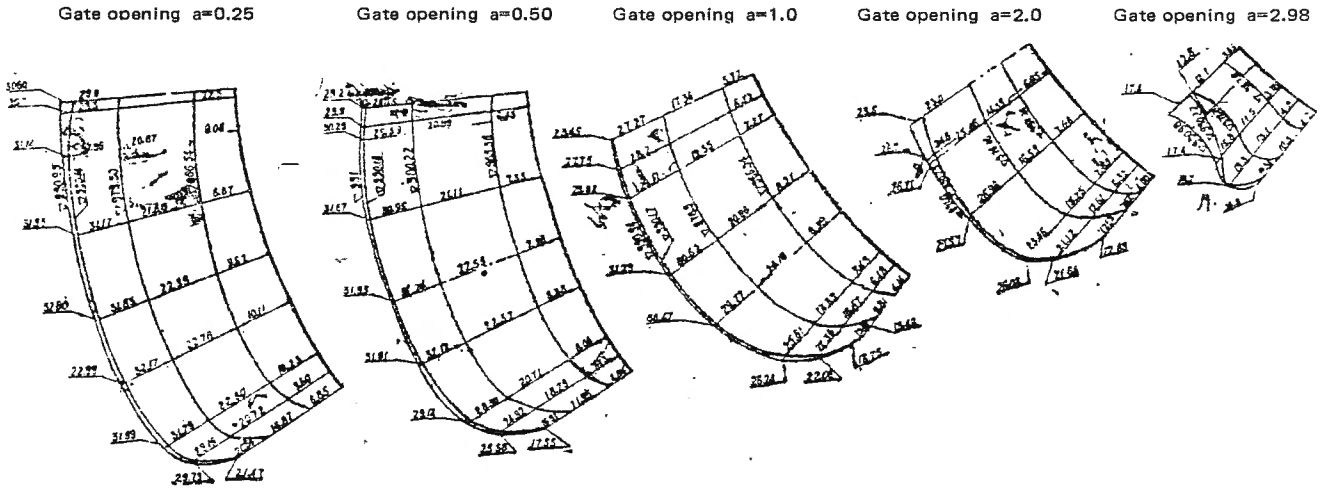

Figure 4. Time-averaged pressure distribution on the gate surface.

Equation (2-4) can therefore be rewritten as

$$P = \gamma H \Phi_5 \ (a/a_i, S/a_i) \tag{2-5}$$

and the time-averaged total pressure P acting on the gate may be expressed as

$$P = \int_s \gamma H \Phi_5(a/a_i, S/a_i) ds \tag{2-6}$$

P is a function of a and H, as shown in Figure 5. Under our experimental conditions there exists the following empirical relationship:

$$P(a,H) = k(a)[H - h(a)] \tag{2-7}$$

where

$$k(a) = 20.850 - 5.833a;$$

$$h(a) = -12.500a^2 + 31.966a + 45.453$$

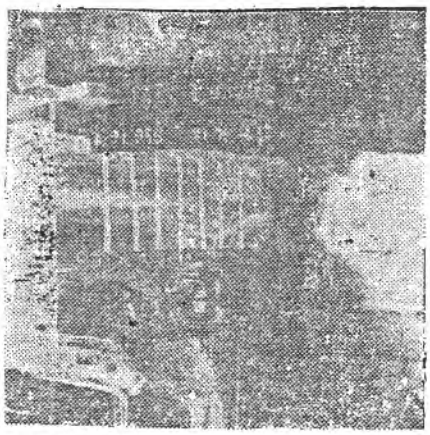

Photo 3

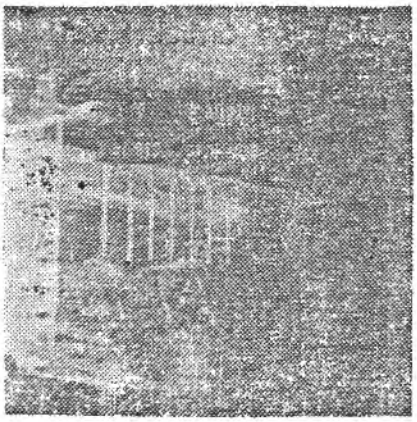

Photo 4

Table 1 shows the experimental data and the calculated results using (2-7). The units of H and a in (2-7) are in meters, and the calculated P is in tons. As can be seen, the agreement between the experimental and calculated values is reasonably good. The errors are greater for a large opening mainly because of the small number of pressure tubes and some of the pressure tubes also malfunctioned.

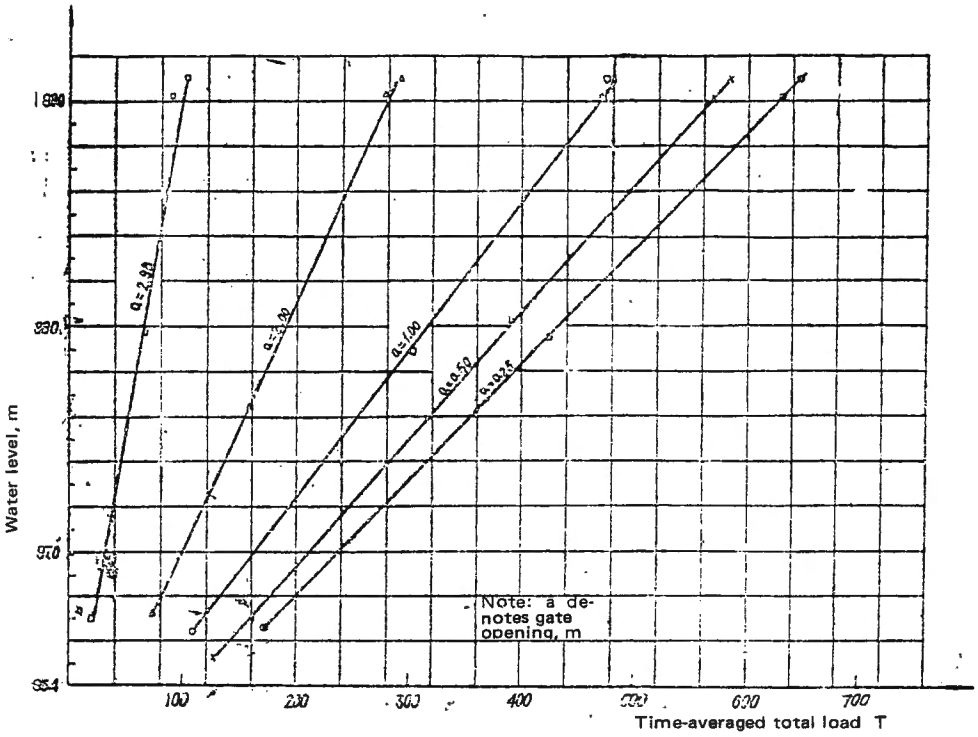

Figure 5. Relationship between reservoir water level and time-averaged total load.

Table 1. Total load P

Opening a. (m)	Calibration water level			Design level			Medium level			Low level		
	Water head H (m)	P (tons)		Water head H (m)	P (tons)		Water head H (m)	P (tons)		Water head H (m)	P (tons)	
		Exp.	Cal.		Exp.	Cal.		Exp.	Cal.		Exp.	Cal.
0.25	35.95	645	644.5	35.14	629	628.7	24.50	424	422.4	11.54	172.1	171.1
0.50	36.00	584	587.3	35.16	570	572.2	25.22	391	394.0	10.36	127.5	127.5
1.00	35.94	473	487.3	35.17	472	475.7	23.90	302.5	306.5	11.34	108	117.9
2.00	36.00	292.5	271.2	35.23	279	264.1	21.46	158.3	137.7	12.24	/	/
2.98	35.98	102	84.03	35.22	87.3	81.4	24.76	65.4	45.1	12.00	/	/

III. Fluctuating load of water flow

In this section we consider the hydrodynamic load on the gate; whereas in the last section the pressure P (H, a, S) was a function of the opening, water head and position, and was independent of time, in this section P becomes a function of H, a, S and t as well.

For a given gate under a given flow condition, a and H are constants, and P is a function of the position S and time t, P = P(S, t). For a given position on the gate surface, P is a function of time only, and we shall denote [a/] this pressure as P(t).

Using resistive pressure transducers, we measured the electric signal x(t) corresponding to the pressure fluctuation at a given position and under various flow conditions. The time history curves x(t) were recorded with a ray-tracing oscilloscope, as shown in Figure 6. Even for a fixed flow rate, the hydrodynamic pressure also showed random fluctuations with time. In fact, the hydrodynamic pressure is a random function of time and the process is a stochastic or random process. For a random function x(t) it is not possible to predict the value of $x(t+\Delta t)$ at time $t+\Delta t$ from the value x(t) at time t. Using resistance type pressure transducers, we measured the pressure fluctuation $x_i(t)$ at various points on the gate surface and the hydrodynamic load on the entire gate structure. The block diagram of these measurements is shown in Figure 7.

(A) Point pressure fluctuation test

The objective of this test is to assess the magnitude and characteristics of the hydrodynamic pressure being exerted on the various parts of the gate. The transducers have a beam frame structure with a 1 cm diameter emulsion film

---

a/ To be consistent with the analysis to follow, it is more illustrative to write P(t) as $x_i(t)$.

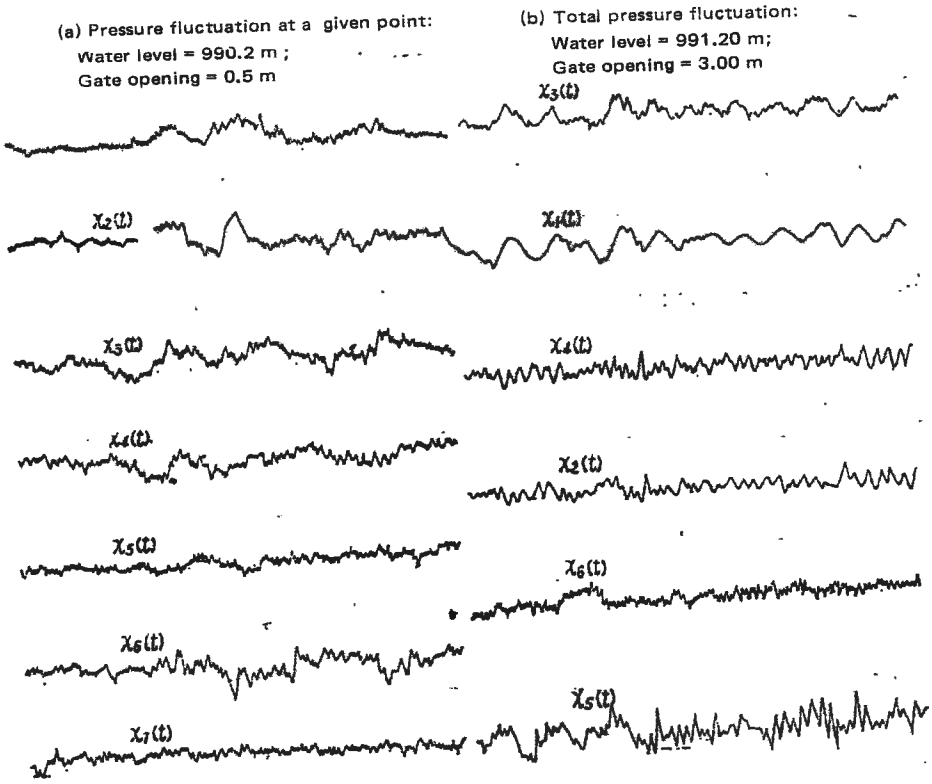

Figure 6. Typical waveforms.

pressure sensing surface. The transducers were installed on the surface facing the water flow and on the bottom of the flume. The locations are shown in Figure 2 and the experimental situation is shown in Photo 5.

(B) Method of analysis

As described above, the pressure fluctuation in a water flow is a random

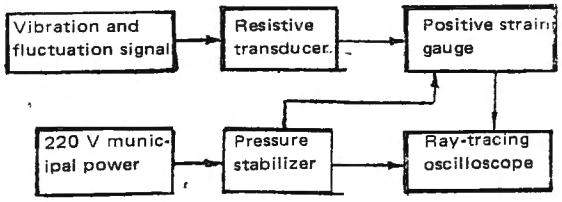

Figure 7. Block diagram of pressure measurements.

process. In the past some artificial criteria were used in processing the

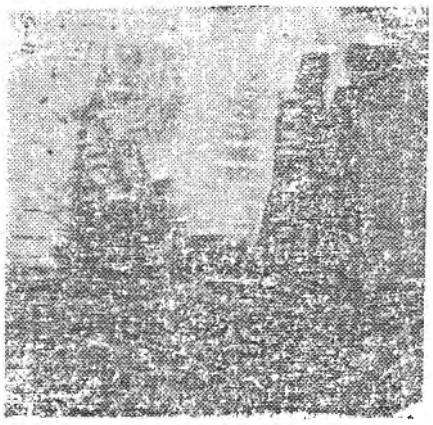

Photo 5. Experimental situation of point pressure fluctuation measurements.

pressure fluctuation data. Using these so-called criteria, the results obtained by even the same person at different times are not the same. Although some statistical approach has been attempted, the emphasis is primarily on frequency analysis to identify the principal frequency, and the method is rather limited in utility.

Recently, some work has been done here and abroad to analyze the load fluctuation in a water flow using the principles of random function. In these studies the frequency characteristics as well as the amplitude characteristics of the fluctuation are analyzed. The variation of the load fluctuation is represented using the statistical characteristics and spectral curves. This appears to be the correct method to treat these fluctuation characteristics.

In general, a process is a stationary random process if all the principal conditions governing the random process are time independent. Specifically, when the flow-controlling conditions such as the structural form, boundary conditions, upstream and downstream water levels, gate opening, and gas flow conditions in the vent pipe do not change with time, the statistical characteristics of the flow will also be time independent. Hence, the statistical nature of the load fluctuation in a fixed-rate (steady) flow under fixed boundary and flow

conditions will be time independent and such a flow may be regarded as a stationary random process. Moreover, experiments have shown that almost all physically meaningful stationary random processes are ergodic.

For ergodic random processes [1-4,6] the reality or sample[a/] average may be replaced by a time average, provided the record is long enough. This would simplify the problem greatly. When the experimental control conditions are held constant and the records are long enough, the process may be regarded as an ergodic stationary random process. The analysis below is based on this assumption.

1. Statistical characteristics

For a random process $x(t)$ fitting the definition above, its statistical characteristics are defined as follows:

(i) mathematical expectation [b/]

$$E\left[x(t)\right]^{*} = \frac{1}{n}\sum_{j=1}^{n} x(t_j) = m_x \tag{3-1}$$

(ii) centralized random variable — A variable is centralized when $x(t_j)$ is replaced by $x(t_j) - m_x$;

(iii) central moments — The second-order central moment is given by

$$\mu_2 = E[\{x(t_j) - m_x\}^2] = \sum_{j=1}^{N} (x_j - m_x)^2/N = \sigma^2 \tag{3-2}$$

The third-order moment is given by

$$\mu_3 = E[\{x(t_j) - m_x\}^3] = \sum_{j=1}^{N} (x_j - m_x)^3/N \tag{3-3}$$

Let the skewness be given by

---

a/ Reality and sample are terms in random function analysis. Here they refer to the results of a given measurement.

b/ The symbol $E[x(t)]$ represents the mathematical expectation of $x(t)$.

Table 2. Statistical characteristics of the point pressure fluctuation

Group	Water level (m)	Opening (m)	Measurement point	Mean square deviation $\sqrt{\mu_2} = \sigma$	Skewness S	Elevation E
201	990.54	0.25	1	1.907	−0.1283359	−0.0609208
			3	6.382	−1.9847646	16.9479708
202	990.25	0.50	1	11.676	0.0647059	−0.1210081
			3	6.336	0.3135012	0.7666556
203	990.25	1.00	1	22.864	−0.0183568	−0.1092382
			3	21.530	−0.4740984	2.7592813
204	990.20	2.00	1	72.656	−0.2996762	1.3828109
			3	232.636	−5.7698778	71.3431713
205	990.12	3.00	1	346.048	0.7406454	0.4791719
			3	270.786	0.5576141	0.3344635
206	983.70	1.00	1	14.256	−0.0612295	0.499651
			3	/	/	/
207	982.32	2.00	1	/	/	/
			3	120.266	0.1205674	0.5928062
208	982.66	3.00	1	214.254	0.9193732	1.9439018
			3	183.060	0.2635439	−0.0962277
209	978.25	0.50	1	7.514	−0.0813285	−0.1777793
			3	/	/	/
210	971.68	1.00	1	9.344	0.0221011	−0.3033328
			3	16.019	−0.0660490	0.3324928
211	971.40	2.00	1	22.743	−0.0178037	0.0105987
			3	85.400	−0.2500915	−0.3777169
212	972.10	3.00	1	110.748	−1.5438206	3.9309072
			3	106.308	−0.7738868	1.2439778

$$S = \mu_3 / \sigma^3 \qquad (3\text{-}3)'$$

The fourth-order moment is given by

$$\mu_4 = E\left[\{x(t_j) - m_x\}^4\right] = \sum_{j=1}^{N} (x_j - m_x)^4 / N \qquad (3\text{-}4)$$

Let the elevation be given by

$$E = \mu_4 / \sigma^4 - 3. \qquad (3\text{-}4)'$$

2. Spectral analysis

(i) Correlation function

$$R_x(\tau) = \frac{1}{n-\tau} \sum_{j=1}^{n-\tau} x(t_j + \tau) x(t_j) \quad \begin{pmatrix} j = 1, 2, \cdots\cdots, n \\ \tau = 1, 2, \cdots\cdots, m \end{pmatrix} \qquad (3\text{-}5)$$

(ii) Spectral density

$$S_x(\omega) = \frac{1}{2\pi} \int_{-T}^{T} R_x(\tau) e^{-i\omega\tau} d\tau \qquad (3\text{-}6)$$

where

$i = \sqrt{-1}$ and $2T$ is the record length.

(C) Test results of point pressure fluctuation

Using the expressions above, we processed the experimental data on a model 719 computer; the results are presented in two parts — statistical characteristics and spectral analysis.

1. Statistical characteristics

The statistical characteristics are certain features of the random variable. The second-order central moment is the degree of scattering of the random variable. Skewness represents the asymmetry of the variable distributions. For a symmetric distribution $\mu_3 = 0$ and $S = 0$, and all the odd-order moments are zero. The elevation represents the sharpness of the peak in the distribution curve; for a normal distribution, $E = 0$. When E is positive, the distribution is steeper than a normal distribution, and when E is negative, the distribution curve is flatter than the normal distribution. The calculated results are shown in Table 2.

2. Spectral analysis

The frequency spectrum and the amplitude of the pressure fluctuation are important inputs to the design of hydraulic structures. In the past, the frequency and the amplitude were analyzed separately, and the actual conditions were not properly addressed. Using spectral analysis, the amplitudes of the fluctuations at all frequencies are displayed in the form of spectral curves, and the frequency range of the peak energy is clearly visible. Spectral analysis therefore can serve as a basis in the analysis of structural vibration.

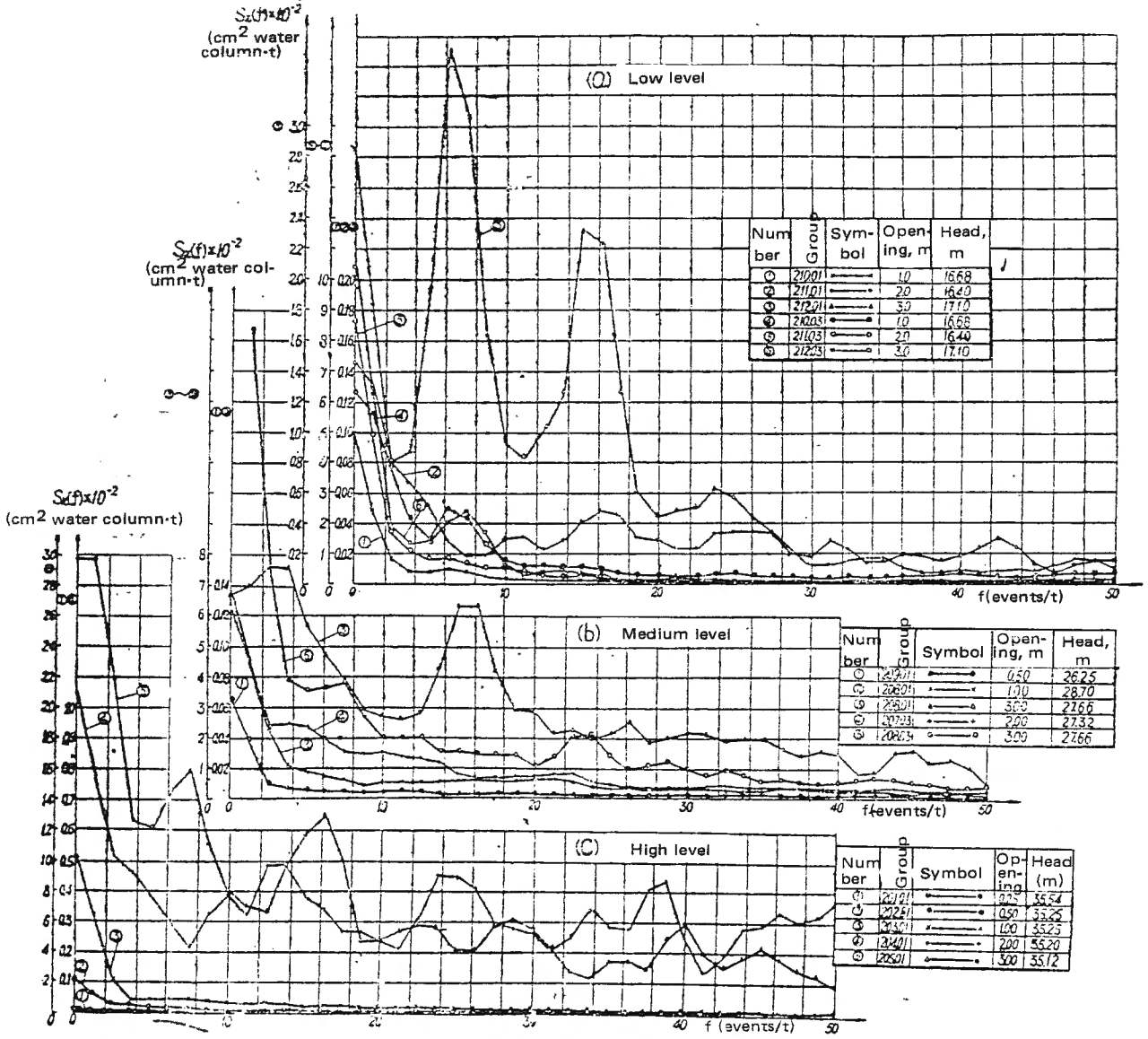

Figure 8. Energy spectra of point pressure fluctuations.

(i) Energy spectrum characteristics

Figure 8 shows the energy spectra of the pressure fluctuation at various points on the gate surface under different flow conditions. The spectral density $S_x(f)$ increases as the opening a increases. For $a \leqslant 1.0$ m, $S_x(f)$ has a maximum at $f = 0$ and gradually decreases with increasing frequency and no other peaks exist in the spectrum. For $a > 1.0$ m, $S_x(f)$ has other pronounced peaks in addition to the one at zero frequency.

It is obvious that the value of $S_x(f)$ increases with water level. The basic features of $S_x(f)$ are the same at different levels, but the peaks become more pronounced at higher levels.

(ii) Distribution of the pressure fluctuation

At a small opening ($a = 0.5$ m), the energy spectrum $S_{xjj}(f)$ of the pressure fluctuation at different positions on the gate surface has a maximum at the bottom edge and the peaks are pronounced. While moving up on the gate surface, the peaks become less pronounced and $S_{xjj}(f)$ also gradually decreases. The following relationship exists:

$$S_{x11}(f) > S_{x22}(f) > S_{x33}(f) > S_{x44}(f) > S_{x55}(f)$$

At a large opening ($a = 2$ m), the distribution characteristics of $S_{xjj}(f)$ are different from those at a small opening. Instead of $S_{x11}(f)$ being the largest, there exists the following relationship:

$$S_{x33}(f) > S_{x22}(f) > S_{x11}(f) > S_{x44}(f)$$

Nonetheless, the characteristics of $S_{x22}(f)$ remain basically unchanged regardless of the opening size.

(iii) Synthesis of pressure fluctuation

In the hydrodynamic consideration of hydraulic structural design, the necessary inputs are the pressure fluctuation and its distribution for a given boundary surface. In fact, the point pressure fluctuation is the random vector acting on a certain point on the gate surface. Imagine that n measurement points are distributed on the gate surface; then the pressure fluctuation may be represented by

$$X_k(t) \qquad (k = 1, 2, \cdots\cdots, n)$$

As before, we assume that $X_k(t)$ is an ergodic stationary random process. The correlation function with respect to time may be written as

$$R_{xkj}(\tau) = \frac{1}{n-\tau}\sum_{j=1}^{n-\tau} X_k(t)X_j(t+\tau) \qquad (k = 1, 2, \cdots\cdots, n) \tag{3-7}$$

For the special case of $j = k$ we have

$$R_{xkk}(\tau) = \frac{1}{n-\tau}\sum_{k=1}^{n-\tau} X_k(t)X_k\ (t+\tau) \tag{3-8}$$

where $R_{xkk}(\tau)$ is the autocorrelation function. $R_{xkj}(\tau)$ is known as the covariant correlation function. The corresponding spectral density is given by

$$S_{xkj}(\omega) = \frac{1}{2\pi}\int_{-T}^{T} R_{xkj}(\tau)e^{-i\omega\tau}d\tau \tag{3-9}$$

where $S_{xkj}(\omega)$ is the covariant spectral density. When $j = k$

$$S_{xkk}(\omega) = \frac{1}{2\pi}\int_{-T}^{T} R_{xkk}(\tau)\, e^{-i\omega\tau}d\tau \tag{3-10}$$

and $S_{xkk}(\omega)$ is the spectral density at point $X_k(t)$

Let the area of $X_k(t)$ be ΔA_k, then the load is

$$X_k(t) \cdot \Delta A_k$$

and the total load P is given by

$$P = X(t) \cdot A = \sum_{k} X_k(t) \cdot \Delta A_k \tag{3-11}$$

where $A = \sum_{k} \Delta A_k$ is the total area of the measurement surface, and $X(t)$ is the average pressure on surface A.

When $\Delta A_k = A/n$

$$X(t) = \frac{1}{n} \sum_{k} X_k(t) \tag{3-12}$$

The correlation functions between $X(t)$ and P are

$$R_x(\tau) = \frac{1}{n^2} \sum_{k} \sum_{j} R_{xkj}(\tau) \tag{3-13}$$

$$R_p(\tau) = \frac{A^2}{n^2} \sum_{k} \sum_{j} R_{xkj}(\tau) \tag{3-14}$$

and the energy spectrum for $X(t)$ and P can be expressed as

$$S_x(\omega) = \frac{1}{2\pi} \int_{-T}^{T} R_x(\tau)\, e^{-i\omega\tau} d\tau = \frac{1}{n^2} \sum_{k} \sum_{j} S_{xkj}(\omega) \tag{3-15}$$

$$S_p(\omega) = \frac{1}{2\pi} \int_{-T}^{T} R_p(\tau)\, e^{-i\omega\tau} d\tau = \frac{A^2}{n^2} \sum_{k} \sum_{j} S_{xkj}(\omega) \tag{3-16}$$

Obviously, the spectral density $S_{xkj}(\omega)$ consists of two parts:

when $j = k$, $S_{xkk}(\omega) > 0$;

when $j \neq k$, $S_{xkj}(\omega) \neq S_{xjk}(\omega) \neq 0$;

we have $S_{xkj}(\omega) < 0$ or $S_{xkj} > 0$

and $S_{xkj}(\omega)$ is known as the covariant spectral density.

Using (3-15), we calculated the energy spectrum of the average pressure $X(t)$ and the results are plotted in Figure 9. As can be seen, $S_x(\omega)$ and $S_{xkk}(\omega)$ are similar and the energy is greater near the bottom. The characteristics of the synthetic spectrum $S_p(\omega)$ are also similar to those of the average pressure energy spectrum $S_x(\omega)$. Furthermore, the energy of the average pressure

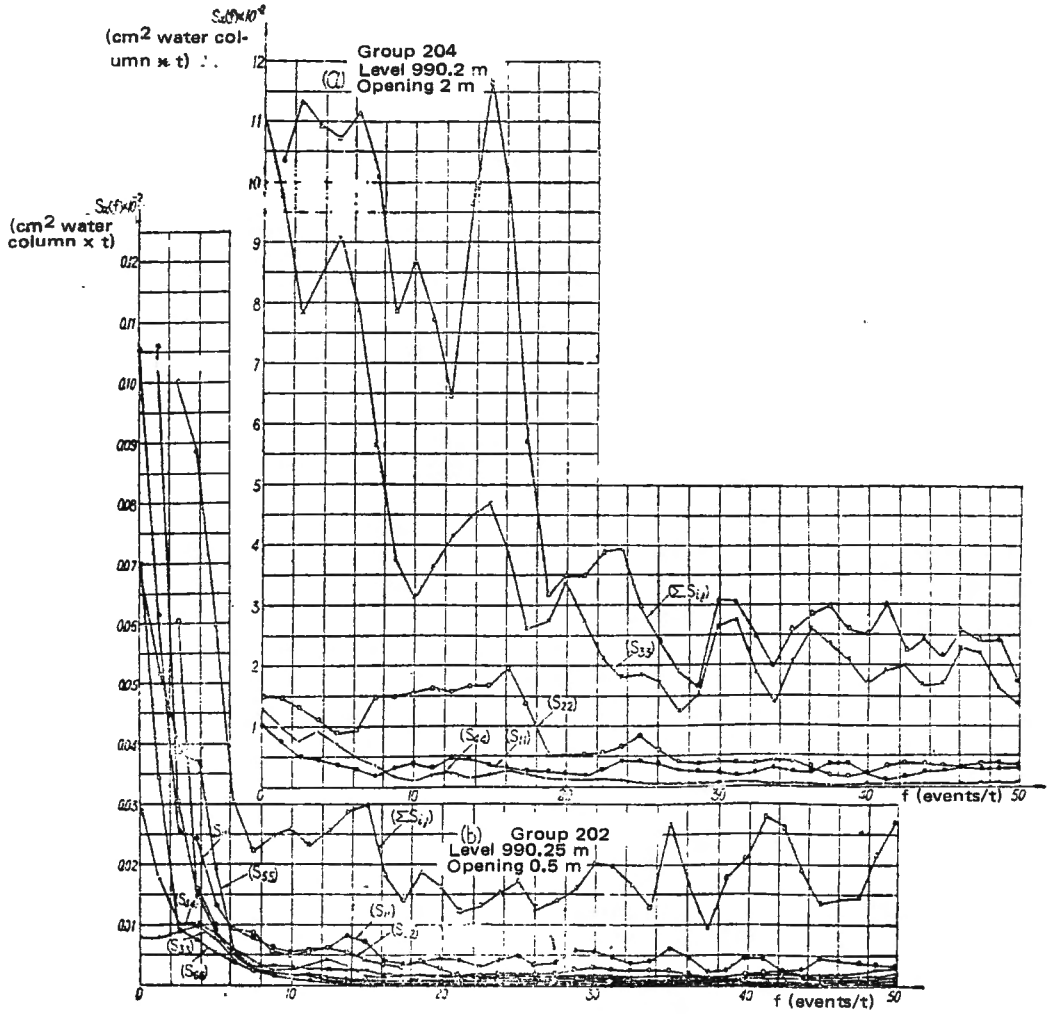

Figure 9. Synthesis of energy spectrum of point pressure fluctuation.

is less than the energy at the bottom edge measurement point but greater than the energy at other points. This is therefore different from the previously held notion that the surface pressure fluctuation is smaller than the point pressure fluctuation.

3. Analysis of fluctuation sources

The pressure fluctuation on the gate plate originates from the upstream fluctuation and can be divided into two parts:

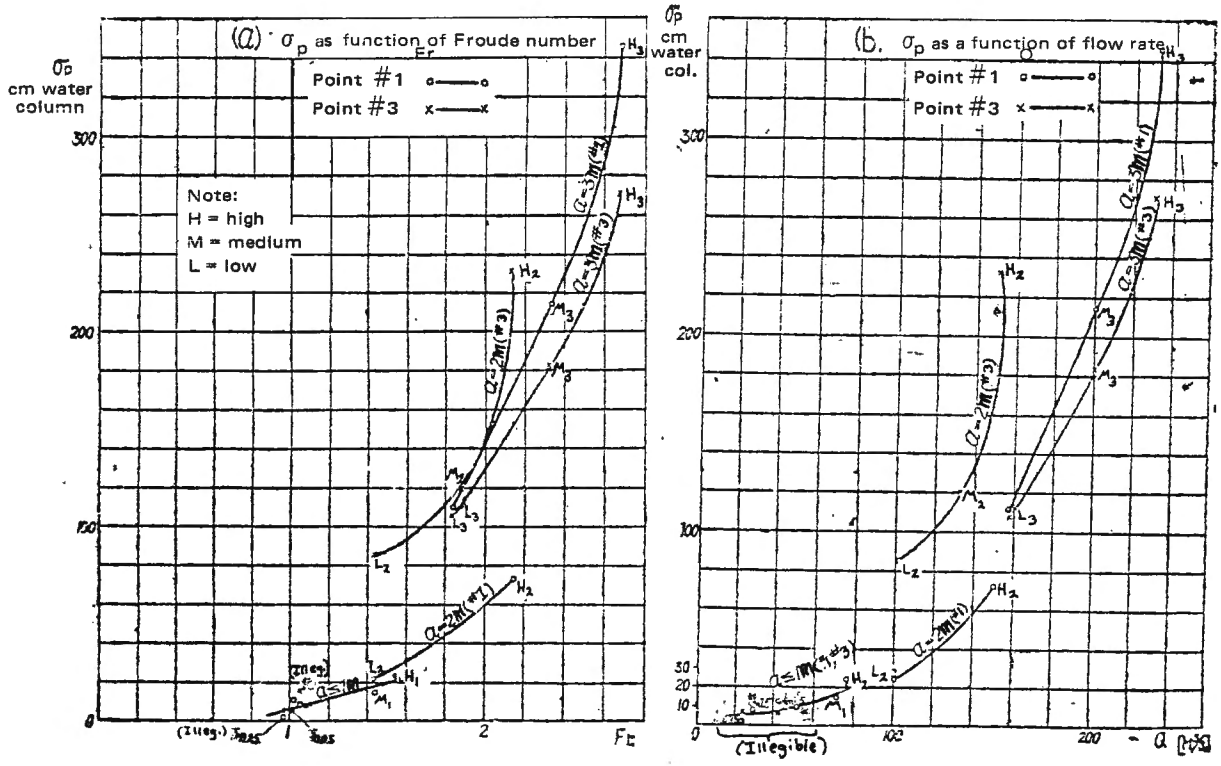

Figure 10. Relationship between the mean square deviation of point pressure fluctuation and the flow parameters.

(i) pressure fluctuations caused by turbulent motion in the flow — The spectrum of this fluctuation is similar to that at small opening and has no obvious peaks. The energy decreases with increasing frequency and on the whole the energy is very small;

(ii) eddy currents produced by nonstreamling boundaries in the upstream — The pressure fluctuation of this source generally has a low frequency, but the energy is much greater than in the previous case. The spectrum has pronounced peaks and the frequency range generally depends on the flow condition.

Figure 10 shows an obvious relationship between the mean square deviation σ_p of the fluctuation and the flow rate Q and the Froude number F_u. The value of σ_p increases as the flow rate and opening increase. For openings greater than a = 1 m, the different boundary conditions corresponding to the

different openings cause considerable differences in σ_p at different locations, as can be seen by comparing #1 and #3 in Figure 10.

4. Summary

For the flow conditions investigated, the source of the point pressure fluctuation on the gate surface is the fluctuation in the upstream flow. The fluctuation energy decreases with increasing frequency, with the frequency range for large energy peaks usually below 20 Hz. The energy is generally small. The synthetic energy spectrum of the point pressure fluctuation may be used to represent the characteristics in a certain range and the energy spectra of the average pressure fluctuation and the total load can be computed. Time correlation is taken into account in such a calculation and consequently the energy spectrum of the average pressure fluctuation is representative of the measurement surface and may be used as an input to the design. Contrary to previous belief, the average pressure fluctuation is not always smaller than the pressure fluctuation at a point, and more data should be collected for further study. Due to the lack of time, we did not work on the modeling of the pressure fluctuation. Since extensive model experiments and on-site observations have shown that the fluctuation frequency is mostly in the 10 to 30 Hz range or even lower, we adopted the conclusion of $\omega_r = 1$ in [8] and accepted the result that $(P/r)_r = L_r$. These choices make the subsequent vibration analysis fall on the conservative side, especially in terms of frequency.

(D) Total load fluctuation test

An understanding of the fluctuation of the total load on the gate is needed in the hydrodynamic design of the support structure and the vibration analysis. In this test we set out to measure the fluctuation of the total load on the gate.

1. Experimental and analytical methods

In the measurement of total hydrodynamic load on the gate, the model not only should resemble the shape of the prototype, the mass and distribution of mass of the gate must also be taken into account so that the motion of the model simulates that of the gate under the hydrodynamic action of the water.

A model design to simulate the gate, shown in Figure 11 and Photo 6, is supported by a specially designed dynamometric system. The action of the supports in this system simulates that of the prototype. The gate is suspended by five dynamometers and two of the hinges are resolved into the vertical and the horizontal components. The structure is configured so that X_1 and X_2 (or X_3 and X_4) do not interfere with each other. At the same time, pressure transducers installed at the bottom of the tunnel measure the pressure fluctuation in the flow.

For a given set of flow conditions there are seven measurement points: $X_1(t)$, $X_2(t)$, $X_3(t)$, $X_4(t)$, $X_5(t)$, $X_6(t)$, and $X_7(t)$.

$X_1(t)$ and $X_3(t)$ are respectively the horizontal force components of the left hinge and the right hinge. $X_2(t)$ and $X_4(t)$ are respectively the vertical force components of the left hinge and the right hinge. $X_5(t)$ is the axial force of the lifter rod. $X_6(t)$ and $X_7(t)$ are the flow pressure fluctuations at the bottom of the tunnel.

Load cells for $X_1(t)$ through $X_4(t)$ are of the steel-ring type, the load cell for $X_5(t)$ is made of organic glass and has a similar design. Point pressure fluctuation transducers are installed at $X_6(t)$ and $X_7(t)$. All the transducers are of the resistance type and work on the same principle as the point pressure fluctuation transducers shown in Figure 7.

The experimental control conditions and the group sequence are the same as before. The measured results represent the components of the hydrodynamic

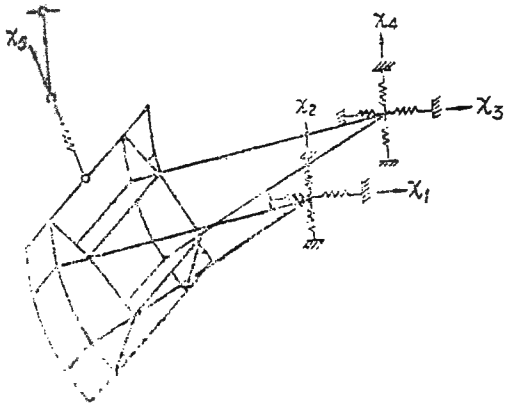

Figure 11. Force measurement system for the total load.

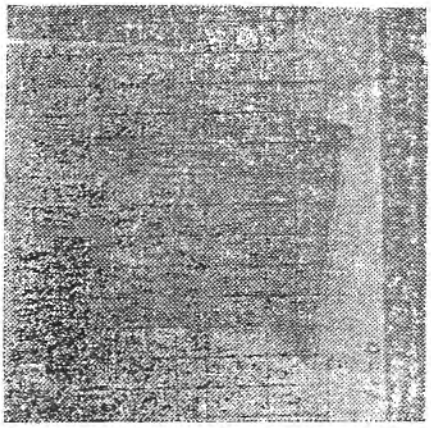

Photo 6. Dynamometer for measuring the total load.

load in the measurement direction. All the $X_i(t)$ are random functions as shown in Figure 6. Moreover, the two horizontal components $X_1(t)$ and $X_3(t)$ and the two vertical components $X_2(t)$ and $X_4(t)$ have the same variation behavior. We shall therefore only analyze the two component forces at one hinge and essentially simplify the problem to a two-dimensional case.

Random functions $X_i(t)$ are taken to be ergodic stationary random processes and the method of analysis is the same as that used earlier for analyzing the point pressure fluctuation.

The resultant force $Z(t)$ acting on a hinge is the vector sum of the horizontal and the vertical components[a/]:

$$\overrightarrow{Z(t)} = \overrightarrow{X_1(t)} + \overrightarrow{X_2(t)} \tag{3-19}$$

By viewing $X_1(t)$ and $X_2(t)$ as two random vectors, the resultant force $Z(t)$ and the corresponding correlation function $R_z(\tau)$ and the energy spectrum density $S_z(\omega)$ have the following relationships:

$$R_z(\tau) = R_{x_1x_1}(\tau) + R_{x_2x_2}(\tau) + R_{x_1x_2}(\tau) + R_{x_2x_1}(\tau) \tag{3-20}$$

$$S_z(\omega) = S_{x_1x_1}(\omega) + S_{x_2x_2}(\omega) + S_{x_1x_2}(\omega) + S_{x_2x_1}(\omega) \tag{3-21}$$

---

a/ The symbol $\overrightarrow{X_j(t)}$ in (3-19) means $X_j(t)$ is a random vector.

2. Statistical characteristics

The physical meaning of the statistical characteristics has already been discussed above. The calculation results are shown in Table 3.

Table 3. Statistical characteristics of the total load fluctuation

Group	Head (m)	Opening (m)	Measure-ment point	Mean square deviation σ_p, tons $\sqrt{\mu_2} = \sigma_p$	Skewness S	Elevation E
108	991.20	3	01	0.480	0.0101114	−0.2208206
			02	2.608	−0.4385695	1.2891971
			03	0.216	−0.3243938	0.1472141
124	980.10	1	01	0.294	0.1506857	−0.2429343
			02	0.940	0.0384696	−0.3132430
			03	0.360	0.2540670	1.9355183
121	991.20	1	01	0.407	−0.1747709	−0.8170879
			02	1.110	0.2386057	1.0561428
			03	0.423	1.2080700	9.1690736
125	980.10	2	01	0.102	0.0657946	0.5648018
			02	0.512	0.2243020	0.3688321
			03	0.448	0.1398881	−0.3457520
16	980.10	3	01	0.240	1.3352727	11.1878977
			02	1.054	0.0701515	0.2026738
			03	0.840	0.0491003	−0.4073212
128	968.30	3	01	0.545	−0.3160464	0.1386427
			02	2.880	−1.1735772	3.2059368
			03	0.990	−0.8222282	0.1824522

3. Spectral analysis

(i) Energy spectrum characteristics

The energy spectra of the total load calculated from the experimental data are shown in Figure 12. This figure shows the effects of water level on load fluctuation. The frequency range at which the energy spectrum $S_x(\omega)$

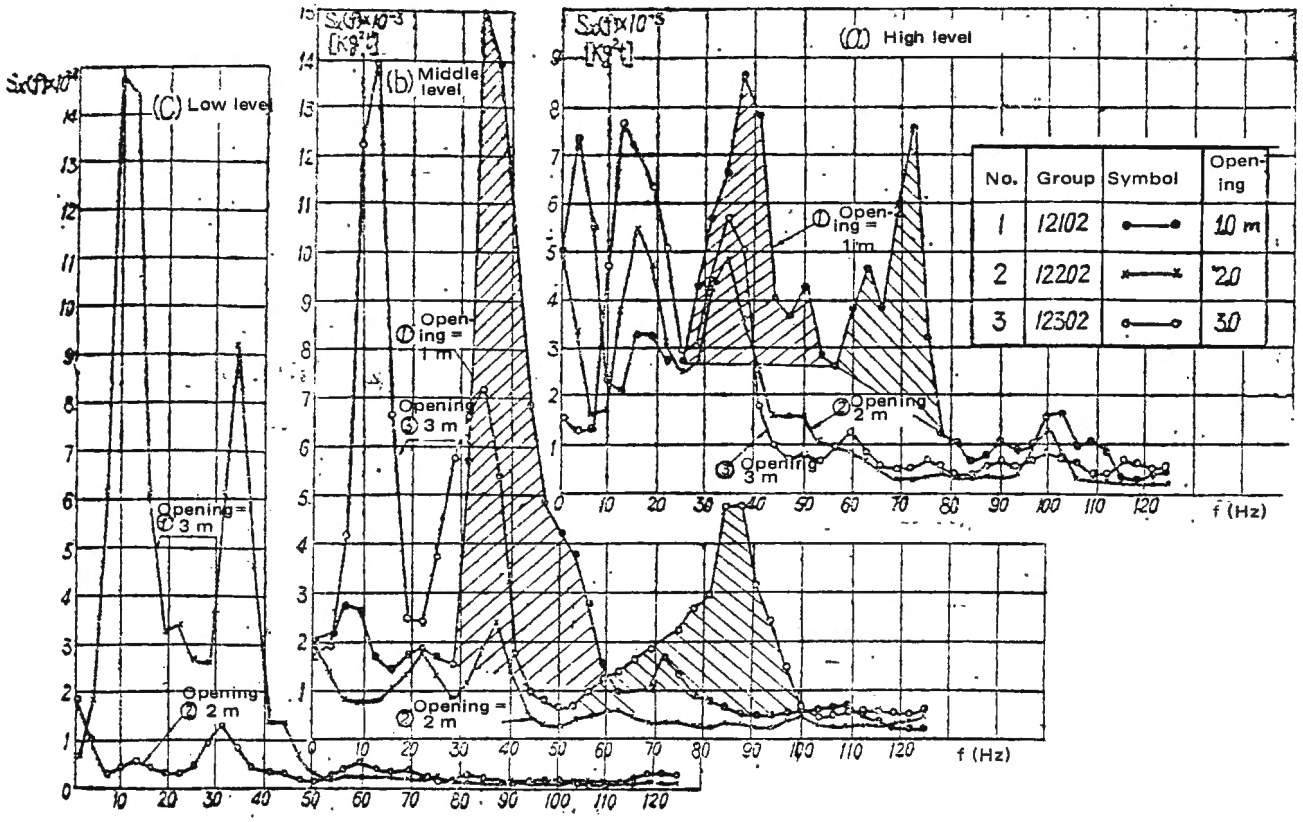

Figure 12. Energy spectra of the load fluctuation.

has a peak does not vary greatly with the opening of the gate. In general, the peak is more pronounced at a greater opening and at a higher water level. This is consistent with the characteristics of the energy spectrum of the point pressure fluctuation shown in Figure 8, the difference being that the load cells used have a low intrinsic frequency and are not ideal for the intended purpose, and the peak corresponding to the resonance between the load fluctuation and the load cell should be taken out, as shown by the shaded area in Figure 12. This effect shows up most strikingly in test group 124 at medium water level and 1.0 m opening. At the same water level, the peak at 35± Hz and an opening of 1.0 m is even higher than that at an opening of 3 m; this is obviously a result of resonance in the measuring device since the self-

oscillation frequency of the load cell in the horizontal direction under these conditions is 39 Hz.

(ii) Effects of the lateral seal

The lateral seal of the gate used in this experiment is a thin rubber sheet installed between the moving gate and the stationary tunnel sidewall. It must be flexible and leakproof. In order to investigate the effects of the seal on the load fluctuation, we removed the seal and recorded the energy spectrum under identical flow conditions. The comparison is shown in Figure 13.

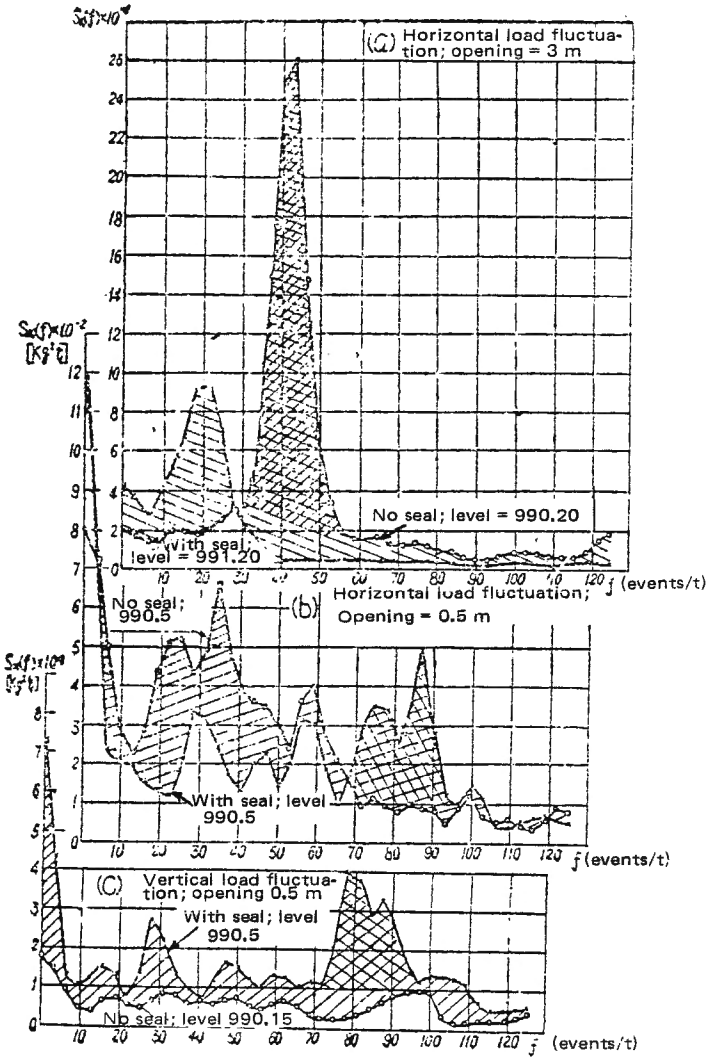

Figure 13. Effects of the lateral seal on the total load fluctuation.

The energy spectra with and without the seal are similar. At an opening of 0.5 m, the energy of the horizontal load fluctuation without the seal is greater than that with the seal, whereas in the vertical direction the energy is smaller [sic] with the seal. At an opening of 3 m, the horizontal load fluctuation with the seal is greater.

The difference in the energy spectrum with and without the seal is shown in Figure 13 as shaded area. This difference is caused by the flow field upstream. The double shaded area in Figure 13 is due to the self-oscillation of the load cell and has been removed in the analysis above.

(iii) Effects of dynamometer sensitivity

In order to study the effects of the load cell stiffness on the energy spectrum, we used four different stiffnesses. The differences in stiffness eventually show up in the sensitivity of the entire force measurement system, including the strain gauge and the oscilloscope. We represent the sensitivity by K in kg/cm and the physical meaning of K is the force (in kg) required to cause a 1 cm deflection of the dot on the oscilloscope. The greater the value of K, the "stiffer" the force measurement system, as shown in Figure 14,a.

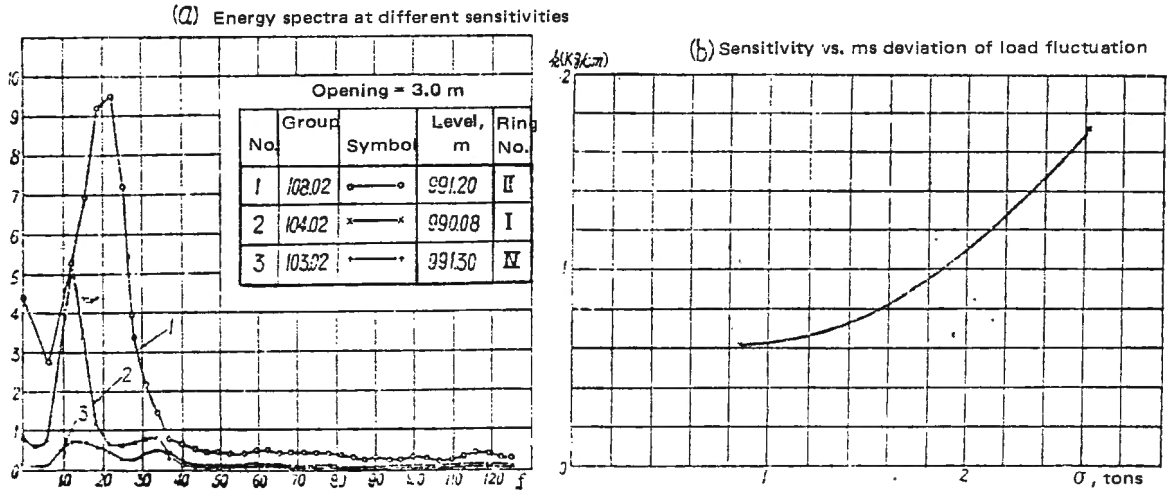

Figure 14. Effects of system sensitivity.

The energy spectra at different K are similar and the spectrum of the smaller K falls within that of a greater K. The greater the K, the higher the spectrum peak.

Figure 14,b clearly shows that the mean square deviation σ of the fluctuation increases with the sensitivity K. In practice the value of K is often chosen to be small; otherwise, the equipment sensitivity would not be enough for the measurement of the needed fluctuation ergodic curve. With inadequate sensitivity, even though the spectrum appears acceptable, the peak values are often too small and do not reflect the actual situation. Even so, such force measurement system is still of value in the experiment.

4. Summary

Experimental results of the total load fluctuation show that the statistical nature and the energy spectrum characteristics of the load are essentially similar to those of the pressure fluctuation at single points. The energy spectra with and without the side seal are basically similar but the energy values are often different. The side seal is generally preferred. The "stiffness" of the force measurement system has a large effect on the energy and especially the peak value of the load fluctuation. The experimental results are therefore useful in optimizing the design plan.

IV. Structural vibration test

The goal of the structural vibration test is to assess the self-oscillation [resonance] characteristics of the gate structure and the lifter rod by performing a model study.

(A) Model design

Similarity criterion in structural vibration: The stiffness and distribution of stiffness of a structure, material properties and forces acting on a structure are similar.

The forces acting on a vibrating structure include inertial force, elastic force and damping force. The similarity criterion requires that forces on the model and prototype be proportional. Inertial force is a body force and depends on the mass density ρ, volume and geometric dimensions of the structure. Therefore, similarity in inertial force is satisfied when the mass density and the mass distribution are similar. The elastic similarity of structures vibrating within the elastic limit is satisfied if the elastic modulus E and G, and in some cases also the Poisson ratio ν, maintain a fixed ratio.

As for the damping force, Coulomb damping is usually considered and similarity should be satisfied by the damping coefficient c and the damping ratio ζ. Due to difficulties in material selection and structural construction, damping is often neglected. Under certain conditions, gravitational similarity must also be considered.

When only elastic and inertial forces are considered in the vibration test, there exists the following law of similarity [7]:

$$f_r = \frac{1}{L_r}\sqrt{E_r/\rho_r} \tag{4-1}$$

Hydrodynamic similarity should ensure that

$$\rho_r = \rho_r' \tag{4-2}$$

where

$$\rho'_r = \frac{\rho_p'}{\rho_m'}$$

and ρ_p' and ρ_m' are respectively the mass density of the prototype and model.

The stiffness of the structure $\overline{y}$ is related to the characteristics and size of the structure and the nature of the vibration. For example, for the bending vibration of a plate we have $\overline{y}_{plate} = \frac{Eh^3}{12(1-\nu^2)}$;

and for the bending vibration of a beam we have $\overline{y}_{beam} = EJ$.

In maintaining the similarity of the major structural components, the following results can be derived from the vibration equation:

longitudinal vibration $$f_r = \frac{1}{X_r}\sqrt{E_r/\rho_r}\ ; \tag{4-3}$$

transverse vibration $$f_r = \frac{1}{X_r^2}\sqrt{\frac{E_rJ_r}{A_r\rho_r}}\ . \tag{4-4}$$

And for lateral vibrations under the action of an axial force we have

$$f_r = \frac{1}{X_r^2}\sqrt{\frac{E_rJ_r}{A_r\rho_r}}\ ; \tag{4-5}_1$$

$$P_r = \frac{E_rJ_r}{X_r^2}\ . \tag{4-5}_2$$

where

x is rod length;
E is elastic modulus for bending;
J is moment of inertia of rod cross-section;
A is cross-sectional area;
ρ is mass density;
P is constant axial force;
f is the resonance frequency of the rod.

Quantities with a subscript r represent the ratios of the physical quantities pertaining to the prototype and the model.

For a normal model, equations (4-1), (4-3) and (4-4) are obviously the same and they serve as the basis for the design of the gate structure. Concerning the lifter rod vibrations, equations (4-5) are used in the model design.

Once the scale L_r and the material of the model are determined, the axial force P is not arbitrary and must satisfy equations (4-5). In our experiment the scale of the model was $L_r = 14$ and the material was organic glass. Since the commercially available organic glass cannot always satisfy the model specifi-

cations, we have made some local changes so that the stiffness distribution of the gate structure satisfies the law of similarity.

(B) Preliminary test

In the determination of the dynamic elastic modulus E_k of the material and the loading method, empirical methods were used on simple components under simple boundary conditions.

1. Selection of components

Simple structural members of different thickness were formed using the organic glass material selected for the model construction. Eight different sizes of flat beams and I-beams were formed.

2. Experimental method

The test piece was held by special clamps and the boundary conditions could be changed by moving the clamp. Resistive strain gauges were attached to the corresponding locations on the test piece to form a half bridge. The strain of the test piece was measured using the resistive strain gauge and an oscilloscope.

When a stationary test piece was subjected to a disturbing force it experienced an initial displacement Δx. When the force was removed, the test piece underwent the classical deformation profile shown in Figure 15. The disturbance

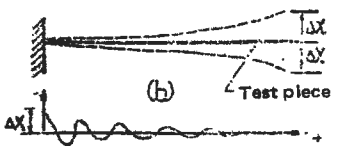

Figure 15. Preliminary test.

can usually be applied in two ways; in the impact method a sudden dynamic force is imparted to the test piece, and in the sudden release method a static force is applied to produce Δx and the static force is then suddenly removed. We used both methods in our experiments.

3. Experimental principle

In the experiment an initial displacement Δx was produced in a given uniform beam and the test piece was allowed to vibrate in the transverse direction under elastic force after the disturbance was removed. For a uniform beam, the vibration frequency is given by

$$\omega_n = a_n\sqrt{\frac{EJ}{ml^4}} \tag{4-6}$$

where m is the mass per unit length;

EJ is the bending stiffness;

l is beam length;

ω_n is the natural frequency and subscript $n = 1, 2....$ corresponds to the mode of vibration;

a_n is a coefficient dependent upon the boundary condition and the vibration mode.

We also know that

$$f_n = \frac{\omega_n}{2\pi} \tag{4-7}$$

In (4-6) and (4-7), m, J, l and a_n are known, and f_n is determined experimentally. The dynamic elastic modulus E_k can then be computed from the equation above.

4. Experimental results

We conducted natural-frequency measurements of the test pieces described above under different boundary conditions; in addition, we repeated the experiments with lead weights glued on the test piece at different separation intervals. The weights of the lead pieces are computed according to the weight of a steel structure of equal dimension.

Three boundary conditions were tested: both ends hinged, both ends fixed,

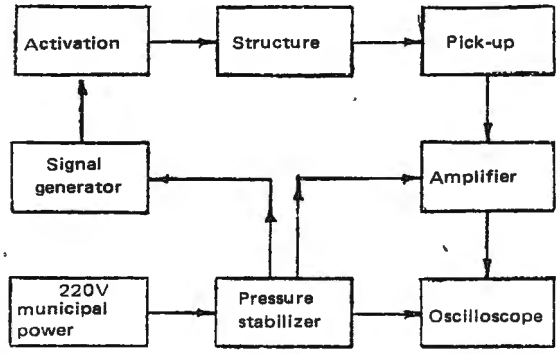

Figure 16. Block diagram of experimental setup.

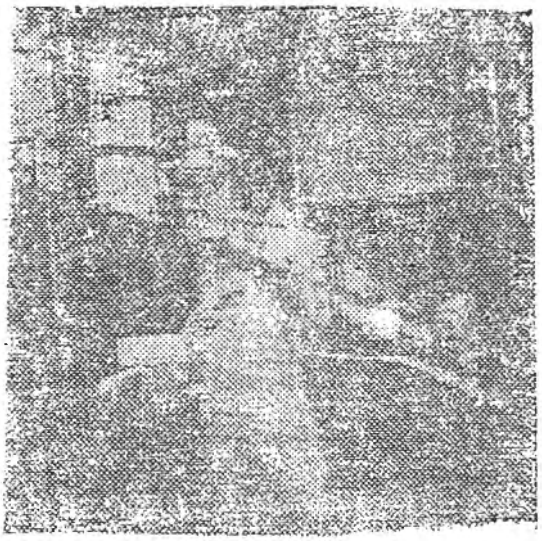

Photo 7. Activated vibration experiment.

and one end fixed with the other end free. The results of the first two cases sometimes deviate from the theoretical prediction. This may be because the test experienced some initial stress when the ends were secured. We therefore used the suspended beam results in computing E_k, the value obtained being greater than E_s. In the model design we used the average of the experimental results and set $E_k = 4.225 \times 10^4$ kg/cm^2.

The experimental result shows that the loading method not only makes the weight of the structure equal to that of a steel structure, but also keeps the elastic modulus equal to that of the organic glass. The error is generally less than 5%.

(C) Experimental method

Both the impact method and the resonance method were used in the experiment. The former was described above and the resonance method is described below.

It is well known that, for a given mode of vibration, any structure has a corresponding intrinsic frequency. A complex structure has a number of vibra-

tion modes. The frequency corresponding to the fundamental (first-order) vibration is called the fundamental frequency. The impact method usually only produces the fundamental frequency, whereas the resonance method can produce higher orders of vibration.

When the frequency f_p of the (external) perturbing force is close to the intrinsic frequency f_i of the structure, resonance occurs. Because of the

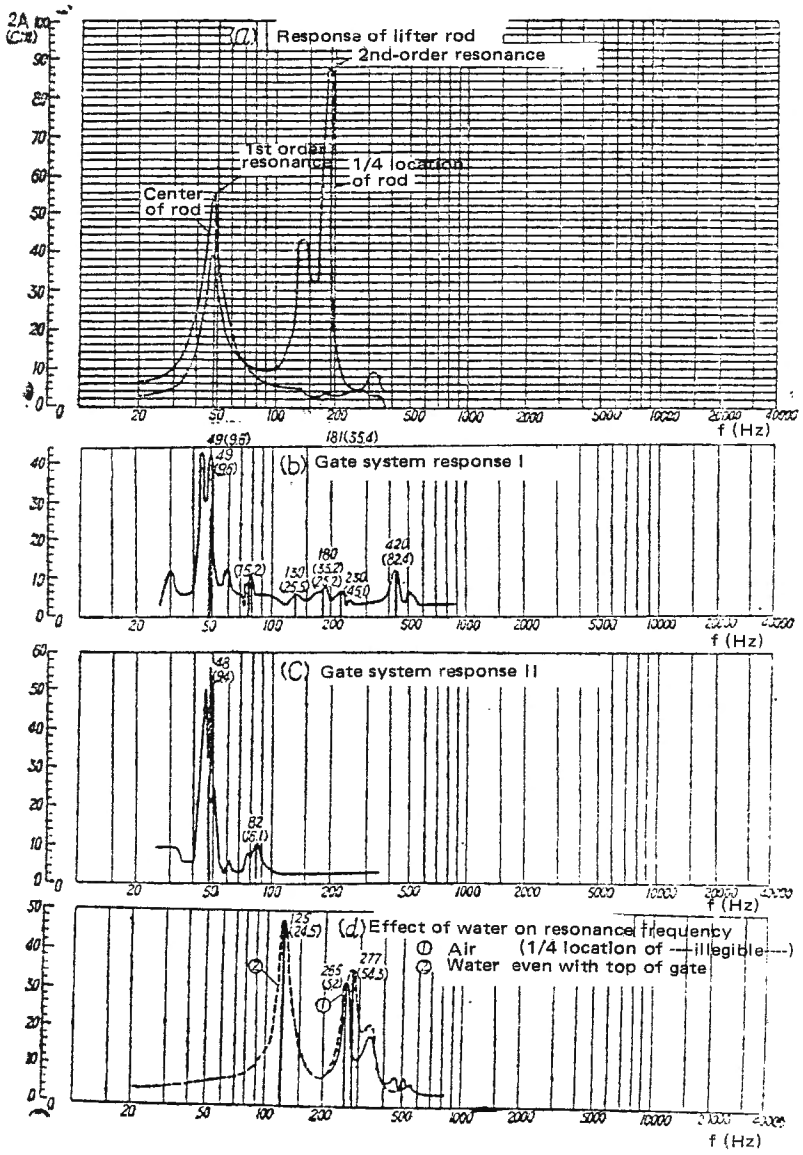

Figure 17. Activation response curves of the gate system.

damping, the structure only produces a larger vibration at resonance and forms a peak.

We used a small home-made[a/] electromagnetic activator as the energy source. The activator transformed the electrical signal of the audiofrequency generator to an alternating disturbance of sufficient frequency bandwidth. When the activator was connected to the structure the alternating force was transmitted to the structure and the structure was set into oscillation.

Resistive films were glued to suitable locations on the gate to serve as pickup sensors, as shown in Figure 2. When the resistors were connected as a bridge circuit, the vibration signals were converted into electrical signals. The resistive strain gauge then displayed the changes on an oscilloscope. The signal generator may be frequency-modulated to vary the frequency of the disturbance over a wide range. When the disturbance frequency approached the intrinsic frequency, the amplitude change of the spot deflection on the oscilloscope was clearly visible. At $f_i \approx f_p$ the structure resonated and the deflection amplitude reached a maximum. The experimental arrangement is shown as the block diagram in Figure 16 and in Photo 7.

Table 4. Values of natural frequencies

Structure		Vibration	First-order (Hz)		Second-order (Hz)	
			Exp.	Cal.	Exp.	Cal.
Lifter rod		Bending	9.2~9.6	8.8	35.2~35.4	35.3
Support arm	X direction	Bending	15.2~16.1	14.7	55.0~58.8	58.8
	Y direction	Bending	45.1~49.0	50.3		204
Beam—support arm combination		π-shaped rigid frame	24.5		53.4~54.3	

a/ Produced by the instrumentation group of the Hydraulics Laboratory.

(D) Test results

1. Resonance characteristics

The arc-shaped gate is a complex three-dimensional structure of rods and may have a number of vibration modes. In the experiment the lifter rod and the gate structure were viewed as a single elastic system and the boundary conditions simulated the actual situation as closely as possible.

Figure 17,a clearly shows that pronounced peaks appear when the activation frequency approaches the intrinsic frequency of the lifter rod. The first peak corresponds to the fundamental frequency and the second peak corresponds to the second harmonic. The vibration mode of the rod at this time is a bending mode. Figure 17,b shows the experimental curve of the gate system, with the peaks corresponding to the various intrinsic frequencies of the gate system. Table 4 shows the experimental results.

The peaks in Figure 17,b give an overall picture of the various resonance frequencies of the gate system. The peak in Figure 17,c shows the first-order resonance in the x direction of a lifter rod of poor stiffness and the support arm. The peaks in Figure 17,d show the first- and second-order resonances of the π-shaped rigid frame formed by the beam system and the support arm. The difference in peak value between the two curves in Figure 17,d shows the effect of water; the presence of water lowers the resonance value slightly.

2. Possible vibration modes of the gate system

In general, a structure of low stiffness is more susceptible to the activation of an external force. In the present system the lifter rod has the least stiffness and is the easiest to activate, especially under impact. Before the installation of the water seals, all the frequencies measured at the test points are close to the resonance frequency of the lifter rod. Among the components of the gate structure, the support arm has the least stiffness and vibrates most easily.

The π-shaped rigid frame formed by the beam system and the support arm is next. The possible modes of vibration are:

a. The gate vibrates as a whole

In the bending vibration of the lifter rod, the gate as a whole moves with the rod and the deformation of the gate is small.

b. Bending vibration of the support arm

The deformation vibration of the support arm is large, whereas the vibration of other members is small.

c. Deformation of the π-structure

The mode of vibration of the combination depends on the energy spectrum of the activation and the characteristics of the structure.

Naturally, the actual vibrations are complicated combinations of a number of modes. From an engineering safety standpoint, the principal modes of vibration should be identified and analyzed.

V. Vibration analysis

The hydrodynamic force on the gate may be resolved into a perpendicular component $Z_0 + Z(t)$ and a tangential component $P_0 + P(t)$. The former is the resultant of the horizontal and the vertical components in the total load test, acting on the gate face and transmitted throughout the gate structure. The latter acts on the lifter rod. Z_0 and P_0 are time independent constant forces and $Z(t)$ and $P(t)$ are time dependent random forces. In the following analysis calculations are performed for the lifter rod and the gate system separately.

(A) Vibration of lifter rod

The vibration of the lifter rod under the action of $P_0 + P(t)$ may be represented schematically as in Figure 18.

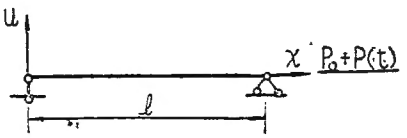

Figure 18. Schematic diagram of the calculation.

The motion satisfies the following equation:

$$EJ\frac{\partial^4 u}{\partial x^4}+\left[P_0+P(t)\right]\frac{\partial^2 u}{\partial x^2}+m\frac{\partial^2 u}{\partial t^2}=0 \tag{5-1}$$

The initial conditions are

$$u(x,0)=u_0,\quad u'(x,0)=u_0' \tag{5-1}'$$

and the boundary conditions are

$$u(0,t)=0,\ u(l,t)=0;$$

$$\frac{\partial^2 u(0,t)}{\partial x^2}=0,\quad \frac{\partial^2 u(l,t)}{\partial x^2}=0. \tag{5-1}''$$

where P_0 is the deterministic axial force;

$P(t)$ is the random axial force;

$u(x, t)$ is displacement;

E is the elastic modulus of the rod;

J is the moment of inertia of the rod cross-section;

m is the mass per unit length of the rod.

1. Simplification of the equation

To simplify equation (5-1), let

$$u(x,t)=\sum_K u_K=\sum_K \phi_K(t)\,\mathrm{Sin}\frac{k\pi x}{l}\ (k=1,2,\cdots\cdots) \tag{5-2}$$

Substituting (5-2) into (5-1) and simplifying, we have

$$\phi_K''(t)+\omega_K^2\left[1-2\mu_K p(t)\right]\phi_K(t)=0 \tag{5-3}$$

where

$$\omega_K^2 = \omega'^2_K\left(\frac{P_{*K}-P_0}{P_{*K}}\right);$$

$$\omega_K' = \frac{k^2\pi^2}{l^2}\sqrt{\frac{EJ}{m}};$$

$$P_{*K} = \frac{k^2\pi^2}{l^2}EJ;$$

$$\mu_K = \frac{1}{2(P_{*K}-P_0)} \qquad (k = 1, 2, \cdots\cdots);$$

Let

$$\begin{cases} a_K = \omega_K^2; \\ b_K = \left(\frac{k\pi}{l}\right)^2\frac{1}{m} \end{cases} \qquad (k = 1, 2, \cdots\cdots) \qquad (5\text{-}3)'$$

where a_K and b_K are time independent and m and k are parameters dependent upon the rod characteristics, then equation (5-3) may be written as

$$\phi_K''(t) + A_K(t)\phi_K(t) = 0 \qquad (5\text{-}4)$$

where

$$A_K = a_K - b_K P(t) \qquad (5\text{-}4)'$$

Thus the problem is converted from solving (5-1) to solving (5-4).

2. Solution of the equation

a. Replacing $A_K(t)$ with the mathematical expectation of A_K

According to (5-4)' and the definition of the mathematical expectation, we have

$$E[A_K(t)] = a_K - b_K E[P(t)] \qquad (5\text{-}5)$$

That is,

$$m_{AK} = a_K - b_K m_p \qquad (5\text{-}6)$$

By replacing $A_K(t)$ with m_{AK}, equation (5-4) becomes

$$\phi_K''(t) + m_{AK}\phi(t) = 0 \qquad (5\text{-}7)$$

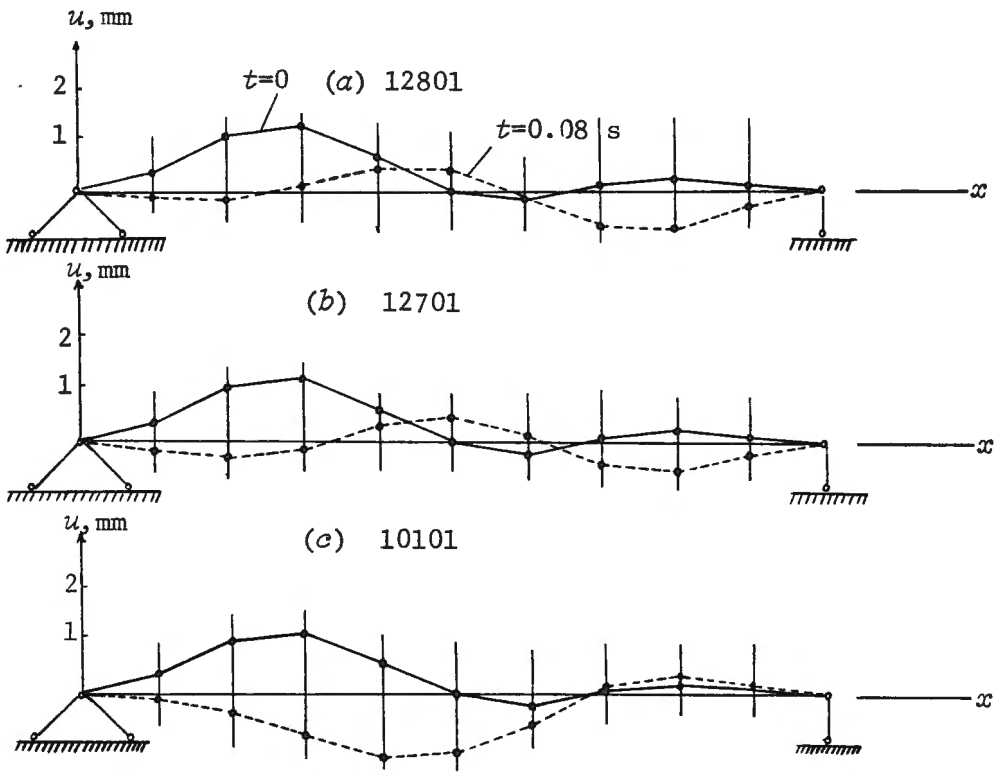

Figure 19. Vibrational displacement of the lifter rod.

Solving equation (5-7) by Laplace transformation, we then obtain the solution of (5-1):

when $m_{AK} > 0$,

$$u(x,t) = \sum_{K} \left[\phi_K(0) \cos\omega_K t + \frac{\phi_K'(0)}{\omega_K} \sin\omega_K t \right] \sin \frac{k\pi x}{l} \quad (k = 1, 2, \cdots\cdots) \qquad (5\text{-}8)$$

when $m_{AK} < 0$,

$$u(x,t) = \sum_{K} \left[\phi_K(0) \operatorname{ch}\omega_K t + \frac{\phi_K'(0)}{\omega_K} \operatorname{sh}\omega_K \tau \right] \sin \frac{k\pi x}{l} \quad (k = 1, 2 \cdots,) \qquad (5\text{-}9)$$

This type of vibration can take place only when one or both of the conditions $\phi_K(0) \neq 0$ and $\phi_K'(0) \neq 0$ are satisfied. Without the water flow, $\phi_K'(0) = 0$. But $\phi_K(0) \neq 0$ may be represented by the following equation

$$u(x, 0) = \frac{qx}{24EJ} (l^3 - 2lx^2 + x^3) \qquad (5\text{-}10)$$

The results of the calculation are shown in Figure 19. As can be seen, the amplitude is not large and the vibration may quickly disappear under the action of damping force.

b. Replace the random function with a cosine function

Let $P(t) \approx P_f \cos\omega_f t$, then substituting into (5-4), we have

$$\phi_K''(t) + (\delta + \varepsilon \cos\omega_f t)\phi_K(t) = 0 \tag{5-11}$$

where

$$\begin{cases} \delta = \left(\frac{k\pi}{l}\right)^2 \frac{EJ}{m}\left[\left(\frac{k\pi}{l}\right)^2 - \frac{P_o}{EJ}\right] \Big/ \omega_f^2 \\ \varepsilon = -\frac{1}{m}\left(\frac{k\pi}{l}\right)^2 \cdot P_f/\omega_f^2 \end{cases} \tag{5-12}$$

Equation (5-11) is a typical Mathieu equation [8]; for some values of δ and ε it has unstable regions, shown as shaded areas in Figure 20,c. The stability of the rod vibration therefore depends on the values of δ and ε. These values depend on the rod property as well as the amplitude and frequency of the perturbation. Since ε is small, we represent the boundaries in Figure 20,c with approximations, as shown in Figure 20,a and b.

We select 6 points from each of the 11 groups of the energy spectrum data $S_p(\omega)$. Using (5-11), the results are calculated on a computer and plotted in Figure 20,a. Only the values of ε and δ for $k = 1$ are plotted, indicating that the rod operates in the stable region. Actually, the value of δ increases considerably when $k > 1$, and the figure shows clearly that the rod is operating in a stable region.

c. Solving the random equation

(i) Solving for the transfer function

Adding a damping term to (5-3), it is rewritten as

$$\phi_K''(t) + 2\zeta\omega_K\phi_K'(t) + \omega_K^2\phi_K(t) = Ae^{i\omega t} \tag{5-13}$$

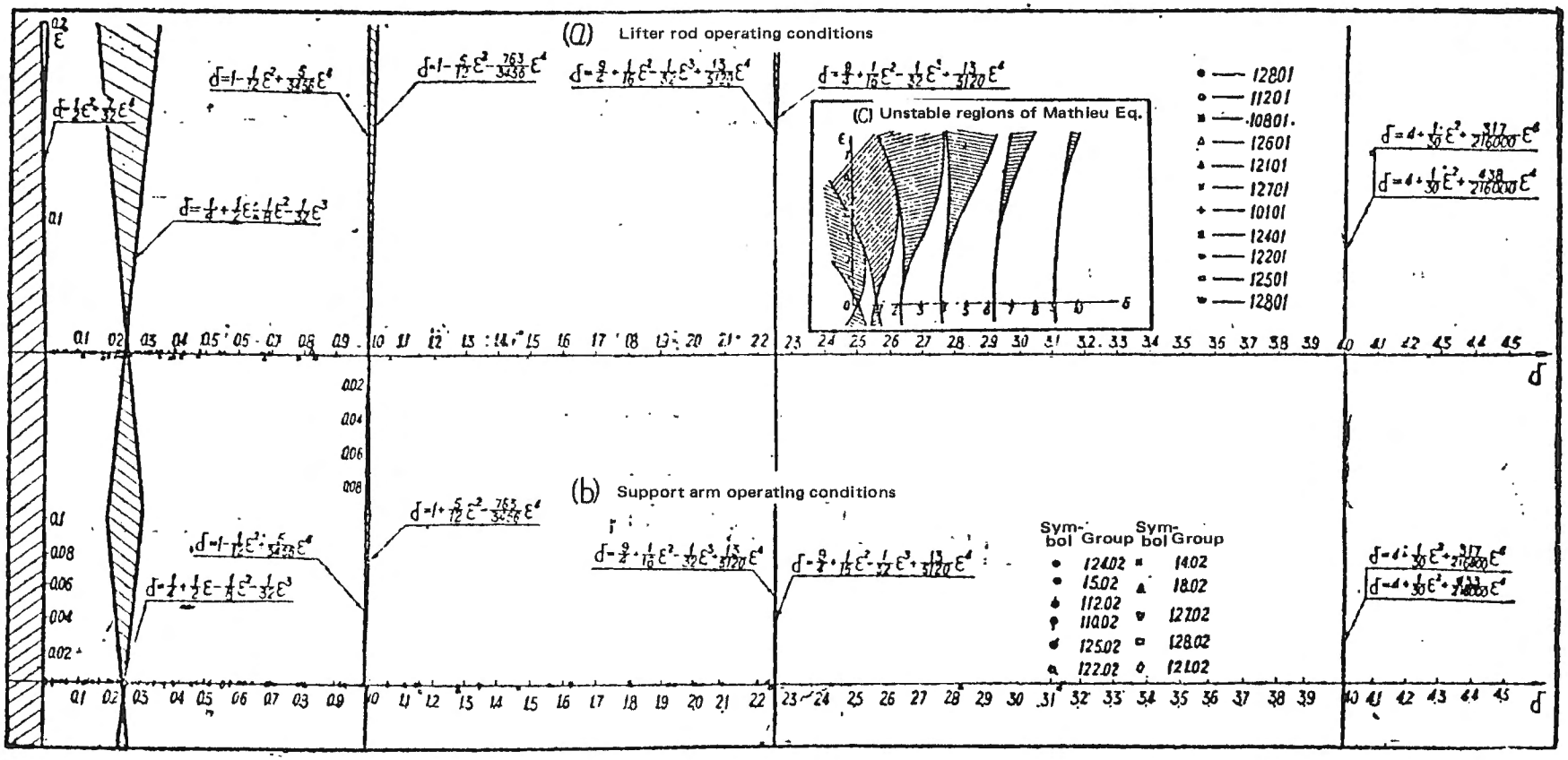

Figure 20. Dynamic stability analysis of the principal components.

Using the Laplace transformation, the transfer function of $\phi_K(t)$ is found:

$$\overline{\phi_K(i\omega)} = \frac{1}{\omega_K^2} \quad \frac{1}{[1-(\omega/\omega_K)^2]+2\xi(\omega/\omega_K)i} \tag{5-14}$$

where $\overline{\phi_K(i\omega)}$ is the transfer function of ϕ_K. The transfer function of $s(x, t)$ is therefore

$$\overline{u(x,\omega)} = \sum_K \quad \frac{1}{\omega_K^2} \cdot \frac{1}{[1-(\omega/\omega_K)^2]+2\xi(\omega/\omega_K)i} \cdot \sin\frac{k\pi x}{l} \tag{5-15}$$

Based on the Wiener-Sinchin [1] equation [2, 6], the energy spectrum of the displacement can be found once the spectrum of the perturbation and the transfer function are known:

$$S_u(x, \omega) = \overline{|u(x, \omega)|}^2 S_p(\omega) \tag{5-16}$$

where $S_u(x, \omega)$ and $S_p(\omega)$ are respectively the spectrum of the displacement $u(x, t)$ and the perturbation $P(t)$.

(ii) Finding maximum bending stress

From structural mechanics [9] we know that the bending moment is

$$M = EJu'' = \sum_K EJ\left(-\frac{k^2\pi^2}{l^2}\right)\phi_K(t)\sin\frac{k\pi x}{l} \tag{5-17}$$

The transfer function of M therefore can be found:

$$\overline{M_K(x, \omega)} = -EJ\frac{k^2\pi^2}{l^2}\ \overline{\phi_K(i\omega)}\ \sin\frac{k\pi x}{l} \tag{5-18}$$

$$\overline{M(x, \omega)} = \sum_K \overline{M_K(x, \omega)} = \sum_K -EJ\frac{k^2\pi^2}{l^2}\cdot\frac{1}{\omega^2_K}$$

$$\frac{\sin\frac{k\pi x}{l}}{[1-(\omega/\omega_K)^2]+2\xi(\omega/\omega_K)i} \tag{5-19}$$

---

[1] Translator's note: unsure of spelling.

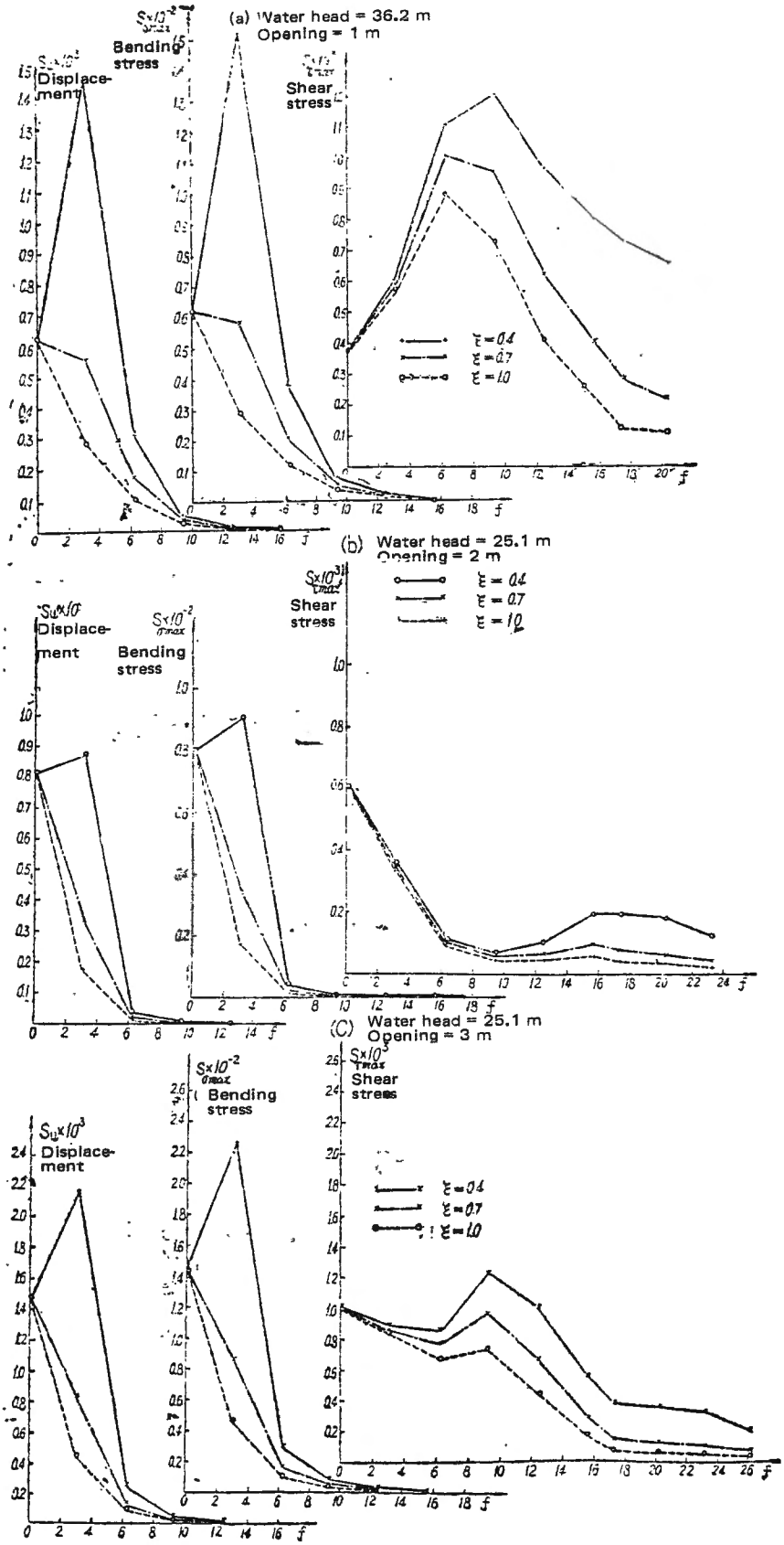

Figure 21. Vibrational spectra of the lifter rod.

Similarly,

$$S_M(x, \omega) = |\overline{M(x, \omega)}|^2 S_p(\omega) \tag{5-20}$$

$$S_{\sigma max}(x, \omega) = |\overline{\sigma_{max}}|^2 S_p(\omega) \tag{5-21}$$

where $S_m(x, \omega)$ and $S_{\sigma max}(x, \omega)$ are respectively the spectrum of the bending moment and the maximum bending stress $\sigma_{max} = \frac{M}{W}$, where W is the cross-section modulus and is equal to J/y_{max}.

(iii) Finding maximum shear stress

The shear force Q and its transfer function $\overline{Q}$ may be represented as

$$Q = \frac{\partial M}{\partial x} = EJ \frac{\partial^3 u}{\partial x^3} = \sum_K - EJ \frac{k^3\pi^3}{l^3} \phi_K(t) \sin \frac{k\pi x}{l} \tag{5-22}$$

$$\overline{Q(x, \omega)} = \sum_K - E\ J \frac{k^3\pi^3}{l^3} \overline{\phi_K(i\omega)} \cos \frac{k\pi x}{l} \tag{5-23}$$

The spectra of the shear force and the maximum shear stress are therefore

$$S_Q(x, \omega) = |\overline{Q(x, \omega)}|^2 S_p(\omega) \tag{5-24}$$

$$S_{\tau max}(x, \omega) = |\frac{4}{3} \frac{\overline{Q}}{\pi r^2}|^2 S_p(\omega) \tag{5-25}$$

where the maximum shear stress is $\tau_{max} = \frac{4}{3} \frac{Q}{\pi r^2}$, and $S_Q(x, \omega)$ and $S_{\tau max}(x, \omega)$ are respectively the spectra of the shear force and the maximum shear stress τ_{max}.

Using the spectra $S_p(\omega)$ of nine sets of experimental forces, we computed the energy spectra of the vibration displacement, the maximum bending stress and the maximum shear stress. The results are given in Figure 21. As can be seen, the magnitudes are all fairly small. Generally, the value below 6 Hz is larger and it decays quickly as the frequency increases. Also, an increase in damping may also cause the spectral peaks to disappear quickly. These results are consistent with the conclusions of the last section.

3. Summary

The analysis above shows that the lifter rod is operating in a stable condition and the magnitude of the flow-induced vibration is small. For the flow conditions studied, flow activation would not cause any danger as long as the material, manufacture and installation are all in accordance with the specifications.

(B) Vibration of gate structure

The vibration modes of the gate are described above. The vibration of the lifter rod analyzed in the last section is really part of the vibrations of the gate as a system. We shall now analyze the possible deformation and vibration of the gate structure.

1. General analysis

The vibration of the gate depends on the energy spectrum of the hydrodynamic force and the structural characteristics of the gate. In addition to the magnitude of the external force, the frequency is an important factor because it directly affects the amplification of the vibration. When the frequency of the perturbation approaches the natural frequency of the structure, the amplification factor becomes large. If there were no damping, the amplification factor would be infinite.

Results of the resonance experiments of the gate structure show that the resonance frequency of the support arm in the x direction is low (15.2 Hz) and the π-shaped rigid frame of the beam system and the support arm has the next lowest frequency and its fundamental frequency is 24.5 Hz.

Relatively speaking, the vibration at 15 Hz contains considerable energy as the amplification at this frequency is large. Therefore, the support arm is more susceptible to vibration and the π-frame is not, because the energy

above 20 Hz is very small. The beam system generally does not have vibration problems because of its high natural frequency. We shall therefore analyze the possible vibrations of the support arm.

2. Vibration of support arm

Treating the support arm as a rod member hinged at two ends, we computed the natural frequency; the results, shown in Table 4, are very close to the experimental values. We can then make use of the diagram in Figure 18 and the analysis method in section (1) to satisfy the equation of motion (5-1). Using equation (5-15), we calculate δ and ε and examine the stability of the operating condition.

Figure 20,b shows the calculated results using the energy spectra $S_X(\omega)$ of 11 sets of forces with 6 data points in each set. Except for a few points located near the boundary of the unstable region, all points are in the stable region. Since the transition from the stable state to the unstable state is critical and the frequency and amplitude of a random external force are only transient, a few points approaching the unstable region is not considered dangerous. Therefore, for the flow conditions studied, there should be no stability problem if the material, manufacture and assembly of the support arm are meeting the quality specifications.

VI. Conclusions

1. The water level and flow rate relationship and the time-averaged pressure distribution on the curved surface of the gate are useful reference data for operation of the gate. The time-averaged total load may be computed from equation (2-7) and the result may be used to assess the force on the hinge.

2. The random fluctuation of the hydrodynamic pressure is analyzed using

the principles of random function analysis. The fluctuation energy obtained from the energy spectrum reflects the behavior of the pressure fluctuation. Under normal flow conditions, the energy of the pressure fluctuation is small; however, the energy below 20 Hz is larger. In this paper we presented, for the first time, a method to calculate the energy spectra of the total load and the average fluctuation from the point pressure fluctuation spectrum and pointed out that the time correlation between the points cannot be ignored. Calculation can be performed using equations (3-15) and (3-16). Such an algorithm can simplify the test facility.

3. In the study of the gate vibration, the lifter, the gate and the water seals should be considered as a single system. The structure is complex and may lead to various modes of vibration. The lifter rod and the support arm have low stiffness and their natural frequencies fall in a region where the flow perturbation has more energy, and so they are therefore susceptible to bending vibration. Using random vibration theory, we analyzed the operating condition and the energy spectra of the displacement, the bending stress and the shear stress. Calculated results show that stability can be maintained in the flow conditions investigated, provided that the material, fabrication and assembly all meet the specifications.

4. The vibration problem of the gate is one of the complex problems in hydraulics and hydraulic engineering, and many questions remain unanswered. Our study is just the beginning. The model we used is not quite large enough and may affect the similarity of the hydrodynamic force near the bottom of the gate. More studies are needed in the future.

REFERENCES

1. Gailulun yu Shulitongji (Probability Theory and Numerical Statistics), Edited by the Mathematics Department, Fudan University, Shanghai Science and Technology Press (Shanghai Kejichubanshe), 1961.
2. Qian Zuesen, Gongcheng Kongzhilun (Theory of Engineering Control), Science Press (Kexue Chubanshe), 1957.
3. Stoke J. J. Nonlinear Vibration in Mechanical and Electrical Systems, Translated into Chinese by Xie Shouxin and Qian Shufu, Shanghai Science and Technology Press, 1964.
4. Otnes Robert K., Enochson Loren, Digital Time Series Analysis, John Wiley and Sons, 1972.
5. Yan Shiwu, Vibration and Lifting Force of Zhangshan Gate in Jiangsu, Nanjing Hydraulic Research Institute, 1972.
6. Robson J. D. An Introduction to Random Vibration, Edinburgh University Press, 1964.
7. Jin Tailai, Vibration of the Canal Head Hinged Gate in Sanyizhai, Second Report, Appendix II: Experimental Test and Calculation of the Resonance Frequency, Beijing Hydraulic and Hydropower Research Institute (Beijing Shuili Shuidian Kexue Yanjiuyuan).
8. Zhao Shijun, Problems in pressure fluctuation in water flow, Shuili Xuebao, Vol. 2, 1959.
9. Xu Zhilun, Wu Yongshen, Engineering Mechanics, Vol. III: Structural Mechanics, Shanghai Xinya Publishing (Shanghai Xinya Shudian).

Acknowledgements

This experimental study began in May 1973 and ended in 1976. In addition to Yan Shiwu, parts of the research were produced by Gao Guangxin, Xu Zhonghe, Li Nanjin, Pi Xiuyun and Wu Jian, as well as Cui Shijun, Chen Xinsun and Xu Guocai of the Xinjiang Hydropower Administration. This report was written by Yan Shiwu.

The computations were performed on the 719 computer in the Computer Center of Tungji University in Shanghai. The Computer Center staff and Qian Meizhen actively supported the computations.

Professors Jin Fulin and Wang Wenliang of the Mathematics Department, Fudan University in Shanghai enthusiastically advised on the computations.

Professor Gu Zhaoxun of the Eastern China Hydraulics Institute provided valuable suggestions on the first draft.

The authors expresses his gratitude to all the people above.